

**FRictional RESISTANCE OF SANDSTONE
FRACTURES UNDER PRE-PEAK CYCLIC LOADING**



**A Thesis Submitted in Partial Fulfillment of the Requirements for the
Degree of Master of Engineering in Civil, Transportation and
Geo-Resources Engineering
Suranaree University of Technology
Academic Year 2018**

ความเสียหายของรอยแตกในหินทรายภายใต้วัฏจักรแรงเฉือนที่ระดับต่ำกว่า
กำลังเฉือนสูงสุด



นายนฤต ปาติตั้ง

วิทยานิพนธ์นี้เป็นส่วนหนึ่งของการศึกษาตามหลักสูตรปริญญาวิศวกรรมศาสตรมหาบัณฑิต
สาขาวิชาวิศวกรรมโยธา ขนส่ง และทรัพยากรธรณี
มหาวิทยาลัยเทคโนโลยีสุรนารี
ปีการศึกษา 2561

**FRICTIONAL RESISTANCE OF SANDSTONE FRACTURES
UNDER PRE-PEAK CYCLIC LOADING**

Suranaree University of Technology has approved this thesis submitted in partial fulfillment of the requirements for a Master's Degree.

Thesis Examining Committee



(Asst. Prof. Dr. Akkhapun Wannakomol)

Chairperson



(Prof. Dr. Kittitep Fuenkajorn)

Member (Thesis Advisor)



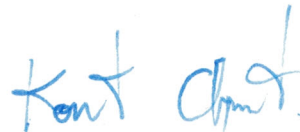
(Assoc. Prof. Dr. Pornkasem Jongpradist)

Member



(Prof. Dr. Santi Maensiri)

Vice Rector for Academic Affairs
and Internationalization



(Assoc. Prof. Ft. Lt. Dr. Kontom Chamniprasart)

Dean of Institute of Engineering

นฤคต ปาติตัง : ความเสียดทานของรอยแตกในหินทรายภายใต้วัฏจักรแรงเฉือนที่ระดับต่ำกว่ากำลังเฉือนสูงสุด (FRICTIONAL RESISTANCE OF SANDSTONE FRACTURES UNDER PRE-PEAK CYCLIC LOADING) อาจารย์ที่ปรึกษา : ศาสตราจารย์ ดร.กิตติเทพ เพ็ญขจร, 72 หน้า.

วัตถุประสงค์ของการศึกษานี้คือ เพื่อหาผลกระทบของแรงเฉือนแบบวัฏจักรภายใต้สภาวะก่อนจุดสูงสุดต่อพฤติกรรมการเฉือนของรอยแตกที่เกิดจากแรงดึงในหินทรายชุดพระวิหาร รอยแตกถูกเฉือนแบบวัฏจักรภายใต้แรงดันไปข้างหน้าและย้อนกลับหลังบนชุดตัวอย่างหินภายใต้ความเค้นตั้งฉากคงที่เท่ากับ 1 2 3 และ 4 เมกะปาสคาล สภาวะการให้แรงแบบ 2 วัฏจักร ได้ถูกดำเนินการภายใต้แอมพลิจูดความเค้นคงที่ และ แอมพลิจูดการเคลื่อนตัวคงที่ ทั้ง 2 สภาวะ ได้ดำเนินการทั้งหมด 50 วัฏจักรการเฉือน ผลการทดสอบระบุว่า การให้แรงแบบวัฏจักรที่สภาวะก่อนจุดสูงสุดสามารถลดค่ากำลังเฉือนและความยืดหยุ่นของรอยแตกในหินทรายได้เล็กน้อย การให้แรงแบบวัฏจักรภายใต้ทั้งสองสภาวะสามารถลดความขรุขระของรอยแตกลำดับที่สอง พลังงานที่ใช้ในการเฉือนรอยแตกเพิ่มขึ้นตามวัฏจักรการให้แรงสำหรับการทดสอบแอมพลิจูดความเค้นคงที่ แต่มีค่าลดลงสำหรับการทดสอบแอมพลิจูดการเคลื่อนตัวคงที่ การทดสอบการเฉือนแบบโมโนโทนิคที่ทดสอบภายหลังการให้แรงแบบวัฏจักรแสดงกำลังเฉือนสูงสุดของรอยแตกว่ามีค่าต่ำกว่ารอยแตกที่ไม่ได้ให้แรงแบบวัฏจักรเล็กน้อย

มหาวิทยาลัยเทคโนโลยีสุรนารี

สาขาวิชาเทคโนโลยีธรณี

ปีการศึกษา 2561

ลายมือชื่อนักศึกษา นฤคต ปาติตัง

ลายมือชื่ออาจารย์ที่ปรึกษา ก. เพ็ญขจร

NARUDON PATITUNG : FRICTIONAL RESISTANCE OF SANDSTONE

FRACTURES UNDER PRE-PEAK CYCLIC LOADING. THESIS

ADVISOR : PROF. KITTITEP FUENKAJORN, Ph.D., P.E., 72 PP.

PHRA WIHAN SANDSTONE/ASPERITY/SHEAR AMPLITUDE/CYCLIC LOADING

The objective of this study is to determine the effect of cyclic loading under pre-peak condition on shearing behavior of tension-induced fractures in Phra Wihan sandstone. Fractures are sheared cyclically under forward and fully backward loading paths under constant normal stresses of 1, 2, 3 and 4 MPa. Two cyclic loading conditions are performed on separate sets of specimens: constant stress amplitude and constant displacement amplitude. A total of 50 shear cycles are applied for both conditions. The results indicate that the pre-peak cyclic loading can slightly reduce shear strengths and stiffness of the sandstone fractures. The cyclic loading under both conditions can degrade the second order asperities of the fractures. The energy required to shear the fractures increases with loading cycles for constant stress amplitude testing, but decreases for constant displacement amplitude testing. The monotonic shear tests conducted after cyclic loading show the fracture peak shear strengths that are slightly lower than those of the identical fractures without cyclic loading.

School of Geotechnolgy

Academic Year 2018

Student's Signature นารุดอน ปาติตุง

Advisor's Signature ค. ฟูเอนคาจอร์น

ACKNOWLEDGMENTS

I wish to acknowledge the funding supported by Suranaree University of Technology (SUT). I would like to express my sincere thanks to Prof. Dr. Kittitep Fuenkajorn for his valuable guidance and efficient supervision. I appreciate his strong support, encouragement, suggestions and comments during the research period. My heartiness thanks to Assoc. Prof. Dr. Pornkasem Jongpradist and Assist. Dr. Akkhapun Wannakomol, for their constructive advice, valuable suggestions and comments on my research works as thesis committee members. Grateful thanks are given to all staffs of Geomechanics Research Unit, Institute of Engineering who supported my work.

Finally, I would like to thank beloved parents for their love, support and encouragement.

Narudon Patitung

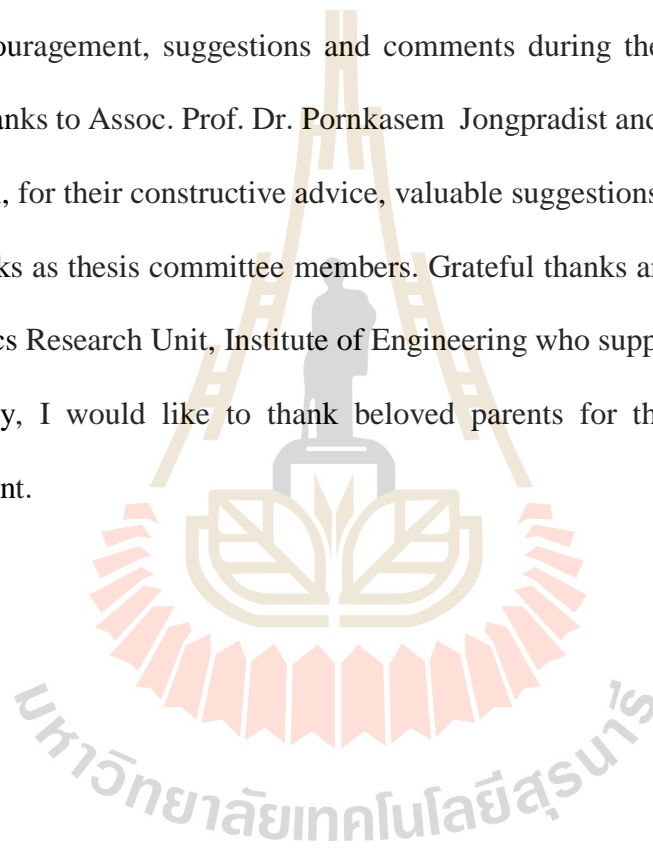


TABLE OF CONTENTS

	Page
ABSTRACT (THAI)	I
ABSTRACT (ENGLISH).....	II
ACKNOWLEDGEMENTS	III
TABLE OF CONTENTS.....	IV
LIST OF TABLES	VII
LIST OF FIGURES	VIII
SYMBOLS AND ABBREVIATIONS.....	XIII
CHAPTER	
I INTRODUCTION	1
1.1 Background and rationale	1
1.2 Research objective	2
1.3 Scope and limitations	3
1.4 Research methodology	4
1.4.1 Literature review	4
1.4.2 Sample preparation and test apparatus	4
1.4.3 Direct shear test.....	5
1.4.4 Cyclic shear loading for constant shear stress amplitude	6
1.4.5 Cyclic shear loading for constant shear displacement amplitude.....	6

TABLE OF CONTENTS (Continued)

	Page
1.4.6 Analysis of test results	8
1.4.7 Discussions and conclusions	8
1.4.8 Thesis writing	9
1.4 Thesis contents	9
II LITERATURE REVIEW	10
2.1 Cyclic shear loading test	10
2.1.1 Cyclic shear loading under control shear stress	10
2.1.2 Cyclic shear loading under control shear displacement	11
2.2 Direct shear test	23
2.2.1 Effects of loading rate on joint shear strength	23
2.2.2 Effect of rock joint roughness on its shear behavior	25
III SAMPLE PREPARATION	30
3.1 Introduction	30
3.2 Sample preparation	30
IV LABORATORY TEST	36
4.1 Introduction	36
4.2 Direct shear test	36
4.3 Cyclic shear test under constant shear stress amplitude	38

TABLE OF CONTENTS (Continued)

	Page
4.4 Cyclic shear test under constant shear displacement amplitude	39
V TEST RESULTS	40
5.1 Introduction	40
5.2 Direct shear test	40
5.3 Cyclic test under constant shear stress amplitude	44
5.4 Cyclic test under constant shear displacement amplitude	49
5.5 Monotonic direct shear test after cyclic loading	54
5.6 Post-test observation	58
VI SHEAR ENERGY	63
6.1 Introduction	63
6.2 Shear energy	63
VII DISCUSSIONS, CONCLUSIONS AND RECOMMENDATIONS FOR FUTURE STUDIES	69
7.1 Discussions	69
7.2 Conclusions	70
7.3 Recommendations for future studies	72
REFERENCES	73
BIOGRAPHY	78

LIST OF TABLES

Table	Page
3.1 Summary of the mechanical properties of rock samples.....	31
3.2 Summary of sample dimensions and their fracture roughness (JRC)	35
5.1 Test variables for constant shear stress amplitude and constant shear displacement amplitude	42
5.2 Peak shear strength after 50 cycle for constant shear stress amplitude and constant shear displacement amplitude	56
5.3 Friction angle and cohesion after 50 cycle for constant shear stress amplitude and constant shear displacement amplitude	56
6.1 Summary of energy for constant stress amplitude	67
6.2 Summary of energy for constant displacement amplitude	68

LIST OF FIGURES

Figure	Page
1.1	Research methodology4
1.2	Direct shear device SBEL DR44 used in this study.....6
1.3	Peak shear strength and forward-backward cyclic shear loading results for constant shear stress amplitude7
1.4	Peak shear strength and forward-backward cyclic shear loading results for constant shear displacement amplitude8
2.1	Failure modes of rock joints in rock samples with multi-level triangular asperities under different number of cycles in the pre-peak cyclic loading tests.....12
2.2	Geometry of damaged asperity surfaces after 20 cycles of sliding for the test reported in photograph of surfaces (a) and sketch of surface shape through a typical cross-section (b)13
2.3	Joint specimens of Hwangdeung granite and Yeosan marble (a) dimension of joint specimen and (b) upper and lower parts of joint specimens16
2.4	Variation of shear strength vs. number of cyclic loading18
2.5	Variations of normalize shear strength against shear rate (first four shear cycles compared)20

LIST OF FIGURES (Continued)

Figure	Page
2.6	Asperity surfaces after 100 shear cycles with shear rate of 5 mm/s: initial normal stress of 0.56 MPa (left), initial normal stress of 2.4 MPa (right).....21
2.7	Shear strengths (τ) as a function of normal stress (σ_n) for peak (a) and residual (b)21
2.8	Shear stress, normal displacement, and normal stress versus horizontal displacement, respectively, on the joint with 15°-15° (a) and 30°-30° (b) asperity angle at normal stresses of 1 MPa23
2.9	Peak (left) and residual (right) shear strengths under various shear rates24
2.10	Area of damage of the joint surface for groups S3 and S4 sheared under different shear rates: area of damage of the joint surface for group S3 (a); and area of damage of the joint surface for group S4 (b).....25
2.11	Three-dimensional reconstruction of the fracture surfaces26
2.12	Direct shear stress test results: shear stress versus shear displacement (a) and shear stress versus dilatancy in relation to shear direction (b).....26
2.13	Comparison of measured and calculated shear failure behavior of single fractures with different surface roughness: (a) friction angle, and (b) failure envelopes29
3.1	Geological map of northeastern Thailand, showing exposure of Phra Wihan sandstone (PWSS) in shade areas.....31

LIST OF FIGURES (Continued)

Figure	Page
3.2	Line load applied at the mid-section of the specimens to obtain a tension-induced fractures (a), and example of tension-induced fractures (b).....32
3.3	Examples of the rock fracture32
3.4	Some tension-induced fractures and their laser scanned images34
3.5	Examples of laser-scanned profiles used to measure the maximum asperity amplitude to estimate the joint roughness coefficient (JRC).....35
4.1	Direct shear device SBEL DR44 used in this study.....37
4.2	Shearing path for constant shear stress amplitude in one cycle38
4.3	Shearing path for constant shear displacement amplitude in one cycle.....39
5.1	Shear stresses as a function of shear displacement41
5.2	Peak and residual shear strength as a function of normal stress41
5.3	Post-test fractures under conventional monotonic shear testing43
5.4	Shear stress-displacement curves for constant shear stress amplitude under normal stresses of 1 MPa (a), 2 MPa (b), 3 MPa (c) and 4 MPa (d).....45
5.5	Fracture shear stiffness (Ks) as a function of shear cycle (N) under normal stresses of 1 MPa (a), 2 MPa (b), 3 MPa (c) and 4 MPa (d).....46
5.6	JRC's of fractures after 50 shear cycles47
5.7	Post-test fractures after 50 shear cycles48

LIST OF FIGURES (Continued)

Figure	Page
5.12 Peak shear strengths as a function of normal stress cycles for constant stress amplitudes (a) and constant displacement amplitude (b). Solid and dash lines are monotonic loading of original fractures and of fractures after cyclic loading, respectively.....	55
5.13 Fracture shear stiffness (K_s) as a function of shear cycle (N) for constant shear stress amplitudes under normal stresses of 1 MPa (a), 2 MPa (b), 3 MPa (c) and 4 MPa (d). Solid and dash lines are monotonic loading results of original fractures and of fractures after cyclic loading, respectively	57
5.14 Fracture shear stiffness (K_s) as a function of shear cycle (N) for constant shear displacement amplitudes under normal stresses of 1 MPa (a), 2 MPa (b), 3 MPa (c) and 4 MPa (d). Solid and dash lines are monotonic loading results of original fractures and of fractures after cyclic loading, respectively.....	58
5.15 JRC's of fractures after monotonic shearing without cyclic loading and after cyclic loading under constant shear stress amplitude (CS) under constant shear displacement amplitude (CD).....	60

LIST OF FIGURES (Continued)

Figure		Page
6.1	Energy (U) as a function of shear cycle (N) for constant shear stress amplitudes under normal stresses of 1 MPa (a), 2 MPa (b), 3 MPa (c) and 4 MPa (d). Solid and dash lines are monotonic loading results of original fractures and of fractures after cyclic loading, respectively	65
6.2	Energy (U) as a function of shear cycle (N) for constant shear displacement amplitudes under normal stresses of 1 MPa (a), 2 MPa (b), 3 MPa (c) and 4 MPa (d). Solid and dash lines are monotonic loading results of original fractures and of fractures after cyclic loading, respectively	66

SYMBOLS AND ABBREVIATIONS

ϕ	=	Friction angle
σ_c	=	Uniaxial compressive strength
σ_n	=	Normal stress
τ	=	Shear stress
τ_A	=	Shear stress amplitude
τ_p	=	Peak shear strength
τ_{post}	=	Peak shear strength under monotonic loading after subjecting to cyclic loading
τ_r	=	Residual shear strength
A	=	Contact area during shear test
c	=	Cohesion
d	=	Shear displacement
d_A	=	Shear displacement amplitude
$d_{n,A}$	=	Normal displacement under cyclic loading
$d_{n,p}$	=	Normal displacement under monotonic loading
$d_{n,post}$	=	Normal displacement under monotonic loading after subjecting to cyclic loading
d_p	=	Peak shear displacement
d_{post}	=	Normal displacement under monotonic loading after subjecting to cyclic loading
JRC	=	Joint roughness coefficient

SYMBOLS AND ABBREVIATIONS (Continued)

K_s	=	Fracture shear stiffness
$K_{s,post}$	=	Fracture shear stiffness under monotonic loading after subjecting to cyclic loading
$K_{s,pre}$	=	Fracture shear stiffness under monotonic loading
N	=	Number of cyclic
P	=	Shear force
R	=	Coefficient of correlation
U	=	Energy
U_A	=	Energy under cyclic loading
U_p	=	Energy under monotonic loading
U_{post}	=	Energy under monotonic loading after subjecting to cyclic loading

CHAPTER I

INTRODUCTION

1.1 Background and rationale

Joint shear strength is one of the key properties used in the stability analysis and design of engineering structures in rock mass, e.g. slopes, tunnels and foundations. The conventional method currently used to determine the joint shear strength is the direct shear testing (e.g. ASTM D5607-08). The joint properties, such as roughness, strength, separation, gouge and even the spatial distributions make the behavior of jointed rock masses more complicated Lee et al. (2001). Most previous laboratory experiments on the mechanical properties of rock joints have been focused on determining the peak shear strength and shear displacement under unidirectional shear loading. Cyclic shearing due to seismic and earthquake loadings can however affect the shear strength. Hosseini et al. (2004) state that small repetitive earthquakes may not make considerable movements, but because of their repetitive nature they may affect the shearing resistance of rock joints. The cyclic effect has been recognized by Hutson and Dowding (1990), Jafari et al. (2003), Mirzaghorbanali et al. (2014) and Kamonphet et al. (2015) who commonly conclude that the cyclic shear loading beyond the peak shear strength can reduce the friction of rock fractures to their residual shear strengths. The cyclic loading can degrade the first and second order asperities along the joint surface and hence reduce its shear strength.

Fathi et al. (2016) and Liu et al. (2018) investigate the shear fatigue damage in rock joints under pre-peak cyclic loading condition. They find that the peak shear strength of fracture decreases with increasing loading cycles. The shear strength of rock joints under cyclic loadings may be an important consideration for long-term stability of engineering structures in the areas where seismic activity and ground vibration occur. Even though the cyclic shear effect beyond the peak shear strength has long been recognized, data basis regarding the effect of the cyclic loading below the peak strength (pre-peak loading cycle) have rarely been produced. In particular, the previous testing has been performed by using one-directional cyclic loading path. Laboratory investigation on the cyclic loading effect under forward to fully backward loading paths has never been conducted. It is presumed in this study that such forward-backward loading path would occur on the rock blocks on mass of rock blocks under in-situ condition where seismic activity occurs.

1.2 Research objective

The objective of this study is to assess the effects of cyclic loading on the frictional behavior of sandstone fractures. The effort primarily involves performing series of cyclic direct shear tests on tension-induced fractures. Two cyclic loading conditions are performed: constant shear stress amplitude and constant shear displacement amplitude. The pre-peak cyclic loading is applied in forward to fully backward manner for both conditions. The fracture shear strength and degradation of fracture asperities under the two cyclic loading conditions are of interest.

1.3 Scope and limitations

The scope and limitations of the research include as follows.

- 1) Laboratory experiments are conducted on specimens of Phra Wihan sandstone.
- 2) All tested fractures are artificially made in the laboratory by tension induced method.
- 3) The test will be used fractures area of $10 \times 10 \text{ cm}^2$.
- 4) Testing on fractures are made under normal stresses from 1, 2, 3 and 4 MPa.
- 5) Two cyclic loading conditions are used: constant shear stress amplitudes and constant shear displacement amplitudes.
- 6) The applied shear stress amplitudes are 25, 50 and 75% of the peak shear strength.
- 7) The applied shear displacement amplitudes are 25, 50 and 75% of the peak shear displacements.
- 8) A total of 50 shear cycles are applied for both conditions.
- 9) Testing procedures follow the relevant ASTM standard practice, as much as, practical.
- 10) The research findings are published in conference paper or journal.

1.4 Research methodology

The research methodology comprises 8 steps; including literature review, sample preparation, direct shear test, cyclic shear stress amplitude, cyclic shear displacement amplitude, analysis of test results, discussions and conclusions and thesis writing. The work plan is illustrated in the Figure 1.1.

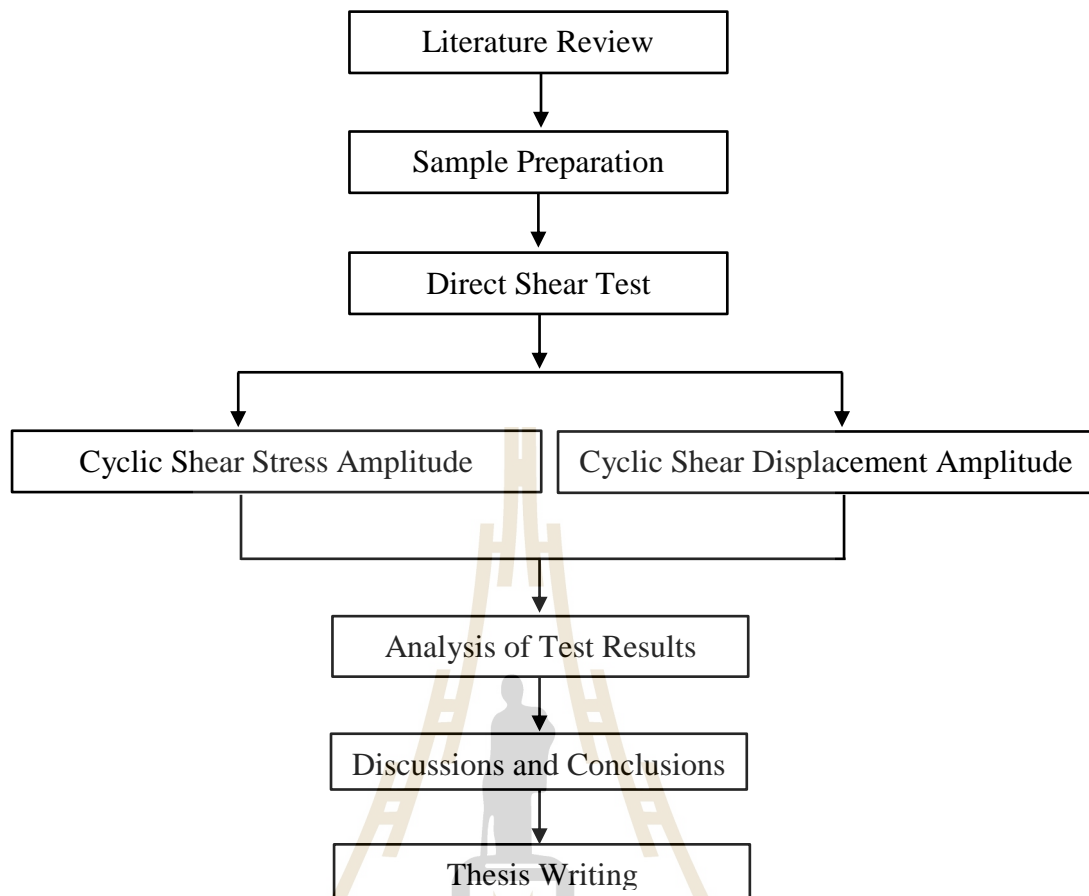


Figure 1.1 Research methodology.

1.4.1 Literature review

Literature review is carried out to understand the shear strength of rock joint under static and cyclic loading. The sources of information are from journals, technical reports and conference papers. A summary of the literature review is given in the thesis.

1.4.2 Sample preparation and test apparatus

The test method and calculation follow as much as practical the ASTM (D5607-08) standard practice. Each specimen is sheared once under each normal stress using a direct shear device (SBEL DR44, capacity of 10,000 pounds normal

load and 30,000 pounds shear force). The rock sample selected for this study is Phra Wihan sandstone. The block specimens is prepared to have nominal dimensions of $10 \times 10 \times 16 \text{ cm}^3$. Specimens with the rough surfaces will be prepared by applying a line load at the mid-section of the specimens until splitting tensile failure occurs (tension-induced fractures). The tested fracture area is $10 \times 10 \text{ cm}^2$. A total of 12 specimens have been tested. Sample preparation is carried out in the laboratory at the Suranaree University of Technology. The specimen is sheared under each normal stress using a direct shear device (SBEL DR44) (Figure 1.2).

1.4.3 Direct shear test

The laboratory testing includes direct shear tests following ASTM D5607-08. The applied constant normal stresses are 1, 2, 3 and 4 MPa. The shear rate is maintained constant at 0.01-0.02 mm/s. The dial gages measure the shear and normal displacements. The direct shear test is determine peak and residual joint shear strength. The test results are shown in forms of the shear strength as a function of normal stress. The peak shear strength is used to calculate the cohesion and friction angle.



Figure 1.2 Direct shear device SBEL DR44 used in this study.

1.4.4 Cyclic shear loading for constant shear stress amplitude

The forward-backward cyclic shear loading test applied constant normal stresses are 1, 2, 3 and 4 MPa. The shear rate is maintained constant at 1 kN/s. A total of 50 cycles is made cycles with the shear stress amplitudes of 25, 50 and 75% of the peak shear strength. The dial gages measure the shear and normal displacements. The loading cycle in forward-backward cyclic shear testing each loading cycle are divided into four stages: forward advance (stage I) to reach the defined maximum stress; return (stage II) to decrease the shear stress to 0 MPa; backward advance (stage III) to reversely increase to the maximum stress; backward return (stage IV) to decrease from the shear stress to 0 MPa. Figure 1.3 shows the comparison the peak shear strength and forward-backward cyclic shear loading results for constant shear stress. The cyclic shear loading shear stress amplitude results are presented in forms of the shear strength as a function of shear displacement.

1.4.5 Cyclic shear loading for constant shear displacement amplitude

The forward-backward cyclic shear loading test applied constant normal stresses are 1, 2, 3 and 4 MPa. The shear displacement rate is maintained constant at 0.01-0.02 mm. A total of 50 cycles is made cycles with the shear displacement amplitude of 25, 50 and 75% of the peak shear displacement. The dial gages measure the shear and normal displacements. The loading cycle in forward-backward cyclic shear testing each loading cycle is divided into four stages: forward advance (stage I) to reach the defined maximum shear displacement; return (stage II) to decrease the shear displacement to 0 mm; backward advance (stage III) to reversely increase to the maximum shear displacement; backward return (stage IV) to decrease from the shear displacement to 0 mm. Figure 1.4 shows the comparison the peak shear strength and

forward-backward cyclic shear loading results for constant shear displacement. The cyclic shear loading shear displacement amplitude results are shown in forms of the shear strength as a function of shear displacement.

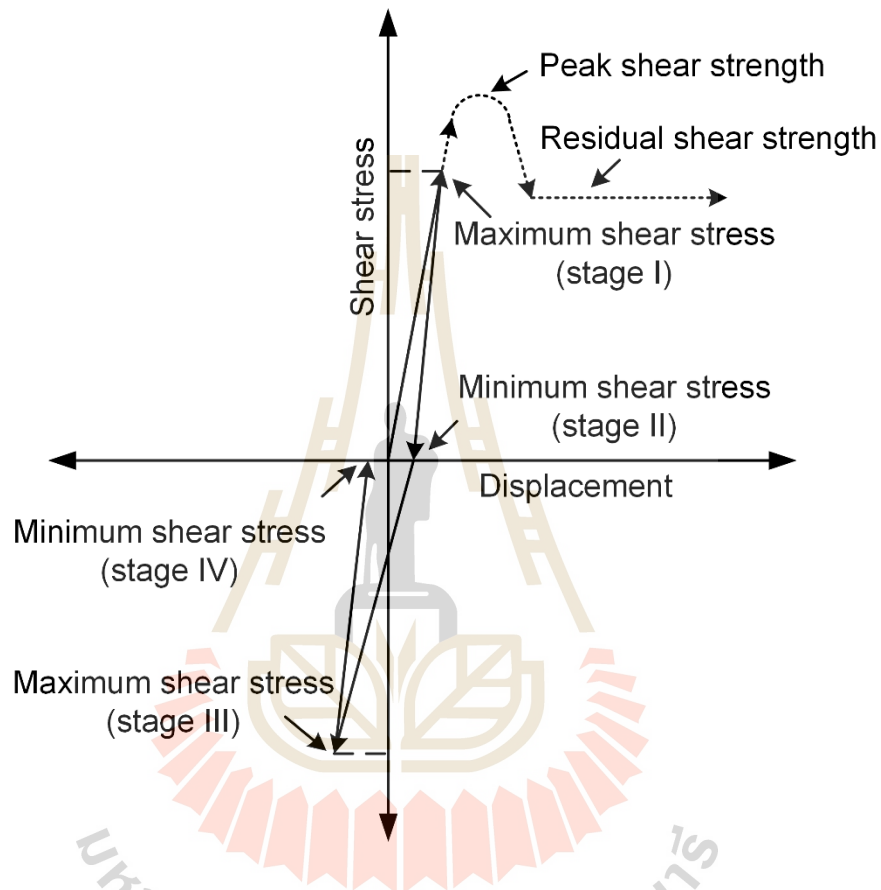


Figure 1.3 Peak shear strength and forward-backward cyclic shear loading results for constant shear stress amplitude.

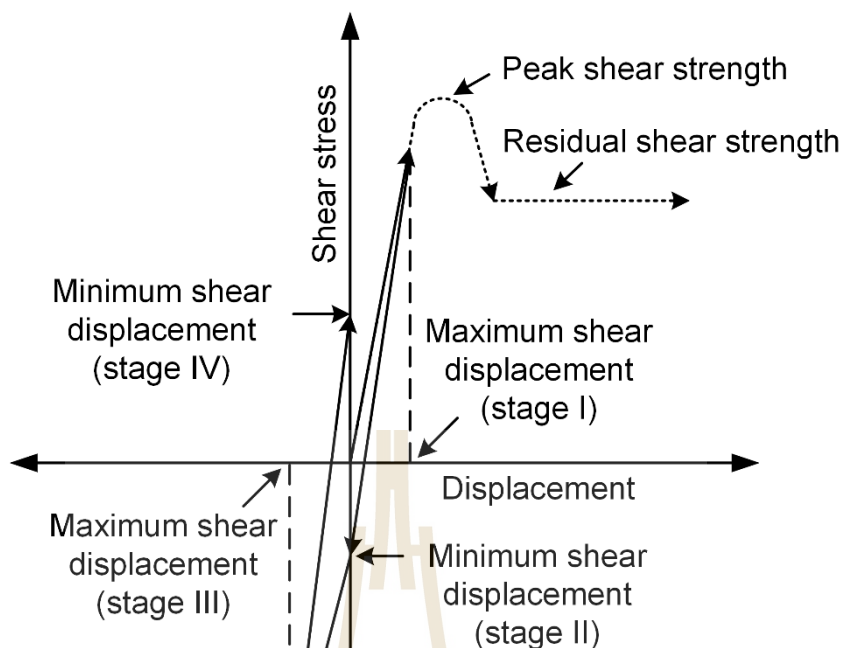


Figure 1.4 Peak shear strength and forward-backward cyclic shear loading results for constant shear displacement amplitude.

1.4.6 Analysis of test results

The analysis of test results describes the three-test series are performed as follows: 1) direct shear test, 2) cyclic shear test under constant shear stress amplitude, and 3) cyclic shear test under constant shear displacement amplitude.

1.4.7 Discussions and conclusions

Discussions are made on the reliability and adequacies of the approaches used here. Future research needs are identified. All research activities, methods, and results are documented and compiled in the thesis. The research or findings are published in the conference proceedings or journals.

1.4.8 Thesis writing

All research activities, methods, and results are documented and compiled in the thesis. The research or findings are published in the journals.

1.4 Thesis contents

This first chapter in traduces the thesis by briefly describing the rationale and background. The second section identifying the research objectives. The third section identifies the research methodology. The fourth section describes scope and limitations. The fifth section gives a chapter by chapter overview of the contents of this thesis.

The second chapter summarizes results of the literature review. Chapter three describes samples preparation. The laboratory tests are described in chapter four. The results of all tests are presented in chapter five. Shear energy described in chapter six. Chapter seven provides the conclusion and recommendations for future research studies.

CHAPTER II

LITERATURE REVIEW

2.1 Cyclic shear loading test

2.1.1 Cyclic shear loading under control shear stress

Fathi et al. (2016) present shear mechanism of rock joints under pre-peak cyclic loading condition. Shear tests are conducted through load-controlled. Load controlled shear tests are conducted under 5, 10, 20, 100, 500, and 1000 cycles of pre-peak loading with amplitudes of 30% and 50% of the maximum monotonic shear strength. The results of the pre-peak cyclic loading tests show that the shear stress increases to 0.25 MPa when the amplitude of cycles was set to 30% of the maximum monotonic shear strength, and increases to 0.42 MPa when the amplitude of cycles is set to 50% of the maximum monotonic shear strength. The shear stress and dilation decrease when the number of cycles increase, while the shear displacement increases. Contraction occurred during low number of cycles, and consequently the contact area and the shear strength parameters slightly increase. During larger number of cycles, degradation occurred on the second order asperities, therefore the shear strength parameters slowly decrease.

Liu et al. (2018) study the shear mechanism of fatigue damage in rock joints with first-order and second-order triangular asperities under pre-peak cyclic loading conditions. A direct shear test is firstly conducted to determine the shear strength in rock samples containing joints with different orders of asperities.

Secondly, influence of the pre-peak cyclic loading conditions with various numbers of cycles on the shear mechanism of fatigue damage in rock joints is studied at constant normal stress. In the cyclic loading conditions, two consecutive steps, such as load controlled and displacement controlled, are applied in tests. The load controlled step is used to achieve the cycles of pre-peak loading in shear tests, and the displacement controlled step is then applied to realize the final failure of rock samples with constant rate of 0.5 mm/min. Moreover, the effects of shear loading rates, numbers of cycle and cyclic shear loading magnitude on fatigue damage, peak shear strength and residual shear strength of rock joints are studied. Fatigue damage occurs at the second-order asperities in the upper and lower blocks within low number of cycles, but the fatigue cracks initiated with initiation angle of 90° with respect to the first-order asperities in the upper and lower blocks coalesce with each other (or rock joints) within the high number of cycles. The variations of peak shear strength and residual shear strength of rock joints within low number of cycles are also different from ones within the high number of cycles, as shown in Figure 2.1.

2.1.2 Cyclic shear loading under control shear displacement

Huang et al. (1993) propose the mechanical behavior of initially closely mated joints in rock undergoing small sliding displacements was undertaken under normal stresses from 0 to 20 MPa. The applied shear displacement amplitude is ± 7 mm. The results obtained indicates that at low normal stresses, surface damage was primarily worn wear which is a gradual process of asperity degradation. At high normal stresses, damage is more rapid and catastrophic in which asperities are sheared.

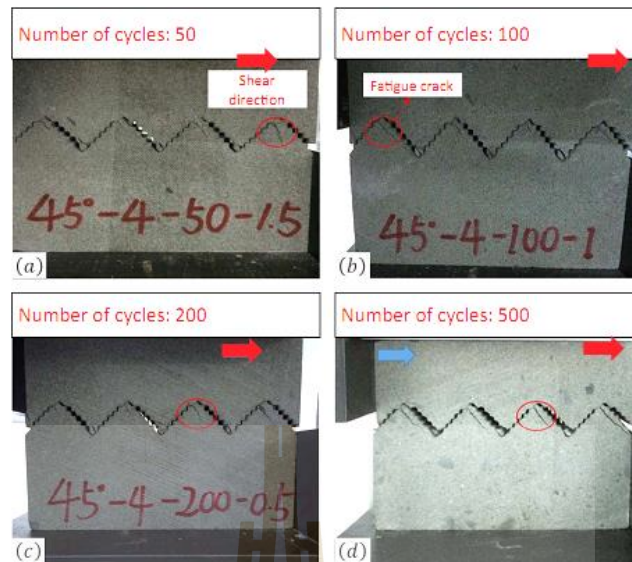


Figure 2.1 Failure modes of rock joints in rock samples with multi-level triangular asperities under different number of cycles in the pre-peak cyclic loading tests (Liu et al., 2018).

At moderate compressive stresses under cyclic sliding conditions, very often the mode of damage was initially wear, with a transition to asperity shearing. It appears that this phenomenon is fatigue-related. The tests also show that the damaged asperity material plays a role in subsequent joint behavior by remaining in the joint, creating a new contact surface and thus modifying the surface shape. Under certain circumstances, such as a cyclic sliding, the asperity debris can migrate depending on the direction of sliding which can give rise to changes in the fully seated position of the joint, as shown in Figure 2.2.

Jing et al. (1993) propose a conceptual model for the behavior of rock joints during cyclic shear and under constant normal stresses according to results from shear tests with 50 concrete replicas of rock joints. The shear strength and deformability of joint samples are found to be both anisotropic and stress dependent. Based on these

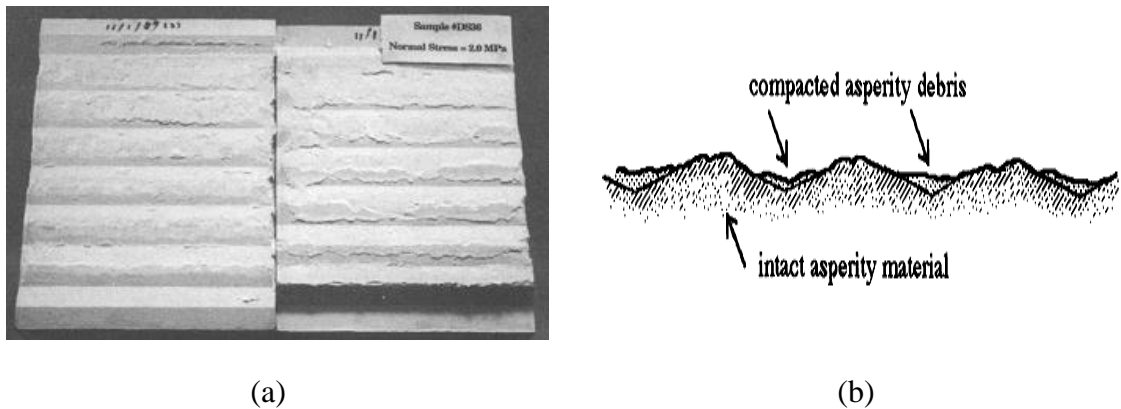


Figure 2.2 Geometry of damaged asperity surfaces after 20 cycles of sliding for the test reported in photograph of surfaces (a) and sketch of surface shape through a typical cross-section (b) (Huang et al., 1993)

experimental results, a two-dimensional constitutive model is developed for rock joints undergoing monotonic or cyclic loading sequences. The joint model was formulated in the framework of non-associated plasticity, coupled with empirical relations representing the surface roughness degradation, appearance of peak and residual shear stresses, different rates of dilatancy and contraction, variable normal stiffness with normal deformation, and dependence of shear strength and deformability on the normal stress. The second law of thermodynamics is represented by an inequality and used to restrict the values of some of the material parameters in the joint model. The new joint model was implemented into a two-dimensional Distinct Element Method Code, UDEC, and its predictions agreed well with some well-known test results.

Souley et al. (1995) investigate joints in a given rock mass that are subjected to a wide variety of boundary conditions and also to various cycles of loading and unloading in both normal and shear directions. Souley et al. (1995) present an extension of the Saeb and Amadei model to take into account joint loading and

unloading in both normal and shear directions. In the normal direction, the cyclic behavior is hyperbolic and the irrecoverable normal closure depends on the joint loading history. Concerning the shear direction change, two assumptions are supposed: the pre-peak behavior is elastic; and, during the residual behavior, the joint is smooth (all the asperities are crushed) and the shear band developed by these fragments is not taken into account.

Ma and Brady (1999) study results from field observations of dynamic behavior of an underground excavation have been compared with numerical studies of the rock deformation history. The field behavior shows progressive accumulation of rock displacement and excavation deformation under successive episodes of dynamic loading. It is possible to reproduce the modes of rock response quite well using a Distinct Element model of the rock mass, but the way displacements develop is dependent on the joint model use in the analysis. It is suggested that, in rock masses subject to repeated dynamic loading, excavation design may need to take account of the prospect of repeated episodes of transient loading at the excavation site.

Homand et al. (2001) propose the mechanical behavior of one artificial granite joint with hammered surfaces, one artificial regularly undulated joint and one natural schist joint was studied. The hammered granite joints underwent 5 cycles of direct shear under 3 normal stress levels ranging between 0.3 and 4 MPa. The regularly undulated joint underwent 10 cycles of shear under 6 normal stress levels ranging between 0.5 and 5 MPa and the natural schist replicas underwent a monotonic shear under 5 normal stress levels ranging between 0.4 and 2.4MPa. These direct shear tests were performed using a new computer-controlled 3D-shear apparatus. To characterize the morphology evolution of the sheared joints, a laser sensor profilometer was used to perform surface data measurements

prior to and after each shear test. Based on a new characterization of joint surface roughness viewed as a combination of primary and secondary roughness and termed by the joint surface roughness one parameter termed joint surface degradation has been defined to quantify the degradation of the sheared joints. Examinations of surface roughness and degradation prior to and after shearing indicate that the hammered surfaces are more damaged than the two other surfaces. The peak strength of hammered joint with zero-dilatancy, therefore, significantly differs from the classical formulation of dilatant joint strength. An attempt has been made to model the peak strength of hammered joint surfaces and dilatant joints with regard to their surface degradation in the course of shearing and two peak strength criteria are proposed. Input parameters are initial morphology and initial surface roughness. For the hammered surfaces, the degradation mechanism is dominant over the phenomenon of dilatancy, whereas for a dilatant joint both mechanisms are present.

Lee et al. (2001) propose a cyclic shear testing system that was established to investigate the mechanical behavior of rough rock joints under cyclic loading conditions. Laboratory cyclic shear tests were conducted for two joint types of Hwangdeung granite and Yeosan marble, as shown in Figure 2.3, saw-cut and split tensile joints. Prior to the test, the roughness of each specimen was characterized by measuring the surface topography using a laser profilometer. Several important aspects of cyclic joint behavior, such as high peak shear strength and non-linear dilation in the first loading cycle, different frictional resistance for the reversed shear loading direction, and anisotropic shear behavior and its dependence on the normal stress level were identified from the cyclic shear test results. These features and their variations in

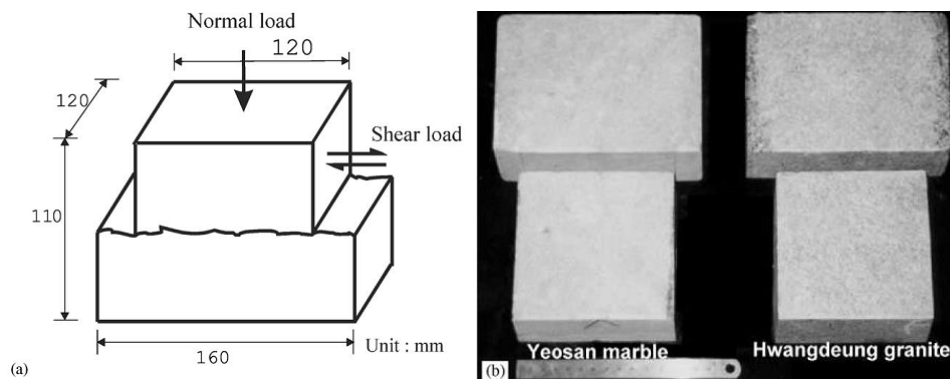


Figure 2.3 Joint specimens of Hwangdeung granite and Yeosan marble (a) dimension of joint specimen and (b) upper and lower parts of joint specimens (Lee et al., 2001).

the subsequent loading cycles were mainly due to the effect of second order asperities and strength of rock material. It was also observed from experimental results that degradation of asperities under cyclic shear loading also followed the exponential degradation laws for asperity angle and the mechanism for asperity degradation would be different depending upon the shearing direction and the type of asperities. Based on the experimental results an elasto-plastic constitutive model, which can consider the degradation of second order asperities, was proposed. Numerical simulations for the monotonic and cyclic shear loading indicated agreement with the laboratory test results.

Puntel et al. (2006) formulate a generalized interface model for joints and cracks in quasi-brittle materials. The proposed model marries an existing fracture mechanics based one developed for monotonic loading of concrete with another frictional based model developed for the cyclic response of rock joints to address the (reverse) cyclic response of rough surfaces in the presence of cohesive stresses is correctly addressed. The properties of the model and its capability to capture several experimentally observed behaviors are shown

by the numerical simulations performed. This joint constitutive model is particularly suitable to simulate the seismic response of dam/rock joints subjected to seismic excitation, or of concrete joints under reverse cyclic loading.

Chern et al. (2012) study the behavior of regular triangular joints under cyclic shearing. Laboratory cyclic shear tests were conducted for three joint types under three different normal stresses, triangular asperities with asperity heights of 6 mm, 4.5 mm and 3.0 mm, respectively, and inclination angle of 22.5°, 17.5° and 12.5°, respectively. All the tests were performed under different initial normal stress (σ_n) of 0.5, 1.0 and 1.5 MPa, respectively. At low levels of normal stress (0.5 MPa), the main shearing mechanism during cyclic shearing is sliding along the asperities. The degradation of asperity continues during cyclic shearing. However, for sample with big asperity height and inclination angle, even at high normal stresses, asperity was not totally broken in the first cycle. All the teeth were cut until the second shearing cycle. As the shear strength is directly related to the dilation angle (i), shear strength will be reduced when the dilation angle decreases (Figure 2.4).

Indraratna et al. (2012) study the cyclic shear behavior of artificial rock joints under constant normal stiffness conditions. To understand the basic mechanisms involved, idealized joint samples were subjected to cyclic loading using a large scale direct shear apparatus for different stress amplitudes. Laboratory cyclic shear tests were conducted on the artificial saw tooth joints with initial asperity angle of 26.5°. Initial normal stresses ranging from 0.16 to 2.64 MPa (0.16, 0.3, 0.56, 1.1, 1.64, and 2.64 MPa) have been applied to the samples. All the specimens were sheared at a constant rate of 0.5 mm/min and under a constant normal stiffness of approximately 7.3 KN/mm. The results obtained indicates that the cyclic shear behavior of the saw tooth joints

under a low level of normal stress ranging from 0.16 to 0.56 MPa. The test results indicate that, at this level of normal stresses, the shearing mechanism after the first cycle is mainly governed by a sliding mechanism with the less pronounced asperity degradation in the consecutive cycles. Nevertheless, asperity degradation is still observed, particularly in the first cycle, and the shear strength diminishes with increasing number of shear cycles. Asperity degradation is evident by the reduction of

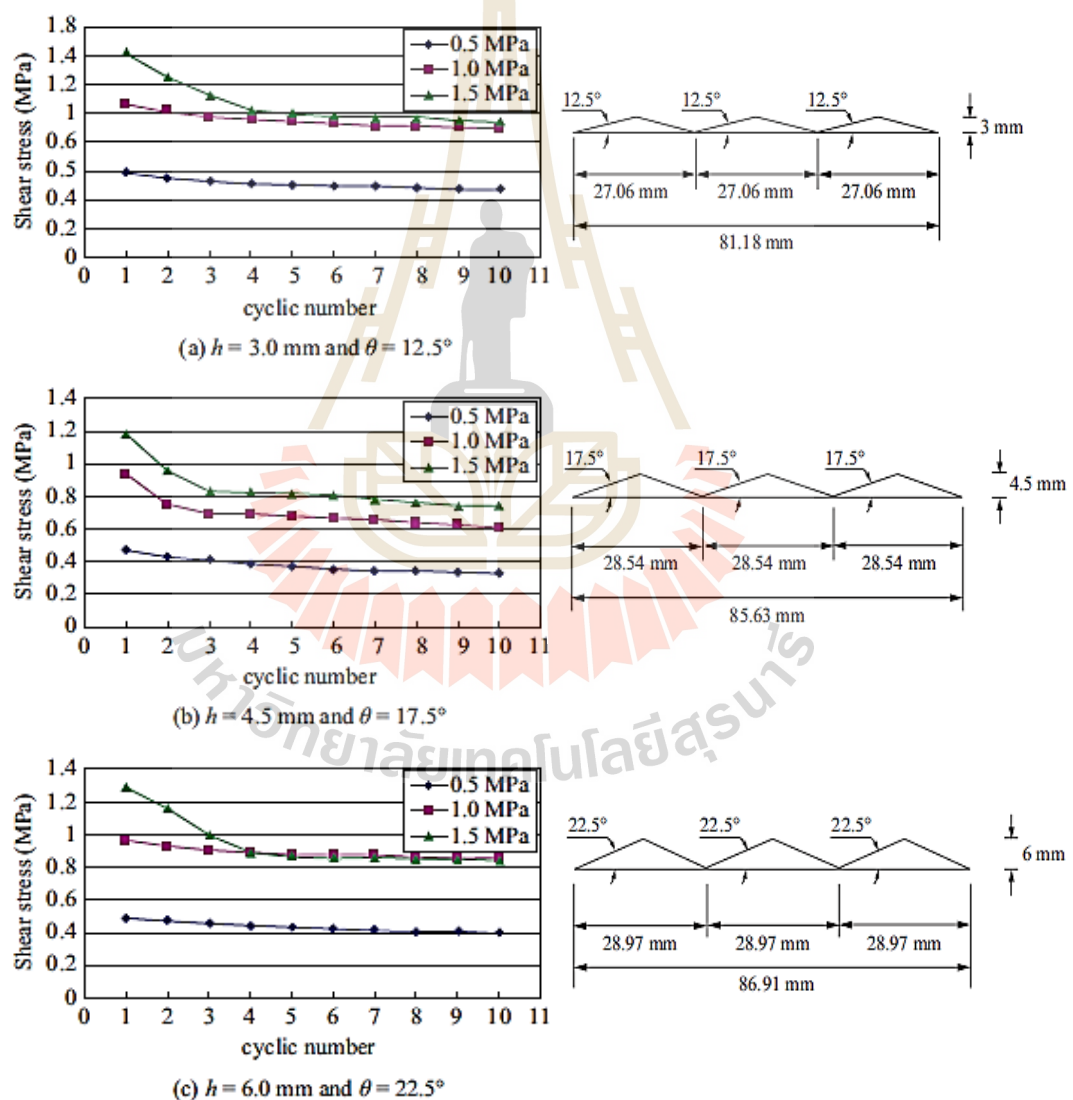


Figure 2.4 Variation of shear strength vs. number of cyclic loading (Chern et al., 2012).

dilation with increasing shear cycles at a high level of normal stress, ranging from 1.1 to 2.64 MPa, the results indicate more pronounced asperity degradation with the shearing mechanism transitioning from a combined sliding and shearing to mainly shearing with increasing normal stresses. This result agrees with Hutson and Dowding (1990).

Mirzaghobanali et al. (2014) study the effects of shear rate on cyclic loading shear behavior of rock joints under constant normal stiffness conditions and normal load. More than nine cyclic loading direct shear tests with shear rates of 0.5 mm/min, 5 mm/s and 20 mm/s and initial normal stresses of 0.56, 1.64 and 2.4 MPa are conducted on the samples. The results obtain that low initial normal stress, the shear strength was higher when overriding the asperities rather than during loading reversal. Due to asperity damage, the shear strength and dilation component decreased with increasing loading cycles. The effect of shear rate on the shear strength when subjected to 0.56 MPa initial normal stress is evident, where an increase in the shear rate from 0.5 mm/min to 5 mm/s resulted in lower shear strength, as shown in Figure 2.5. As the normal stress increased, the effects of shear rate became less pronounced. The surfaces of asperities sheared for 100 loading cycles with 5 mm/s shear rate under 0.56 and 2.4 MPa initial normal stresses are compared in Figure 2.6. It can be noted that, for low value of initial normal stress, asperities were degraded smoothly as shearing proceeded, while for high value of initial normal stress, asperities were sheared off from the base.

Kamonphet et al. (2015) perform a direct shear tests to determine the peak and residual shear strengths of fractures in sandstone, granite and limestone under cyclic shear loading beyond the peak strength. The fractures are artificially made in the laboratory by tension inducing and saw-cut methods. Results indicate that the cyclic shear load can

significantly reduce the fracture shear strengths and stiffness. The peak shear strengths rapidly decrease after the first cycle and tend to remain unchanged close to the residual strengths through the tenth cycle. Degradation of the first order asperities largely occurs after the first cycle. The fracture dilation rates gradually decrease from the first through the tenth cycles suggesting that the second order asperities continuously degrade after the first load cycle. The residual shear strengths are lower than the peak shear strengths and higher than those of the smooth fractures. The strength of smooth fracture tends to be independent of cyclic shear loading, as shown in Figure 2.7.

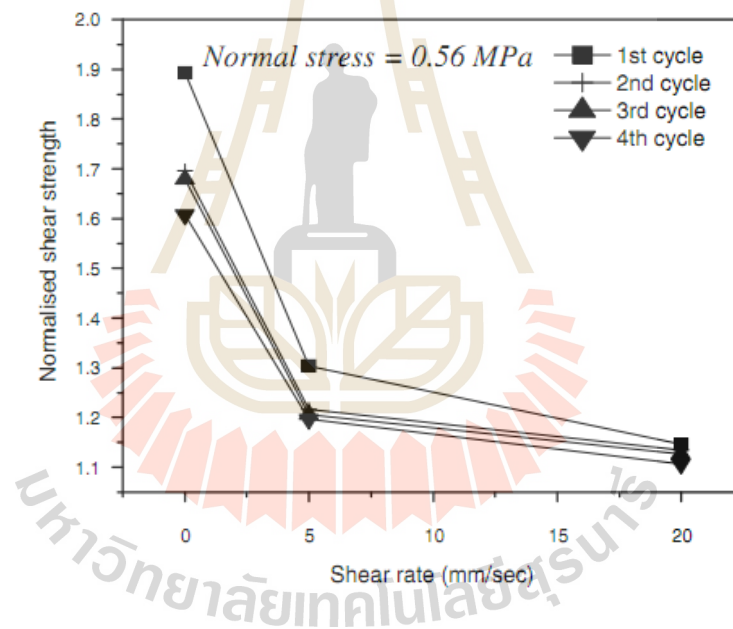


Figure 2.5 Variations of normalize shear strength against shear rate (first four shear cycles compared) (Mirzagherbanali et al., 2014).

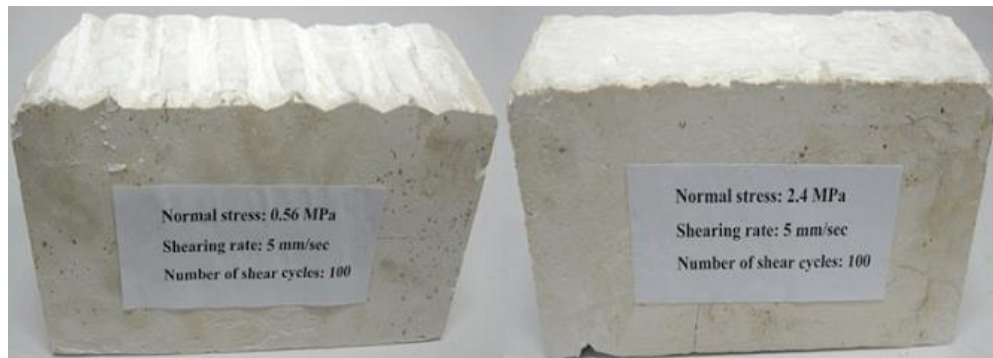


Figure 2.6 Asperity surfaces after 100 shear cycles with shear rate of 5 mm/s: initial normal stress of 0.56 MPa (left), initial normal stress of 2.4 MPa (right) (Mirzaghobanali et al., 2013).

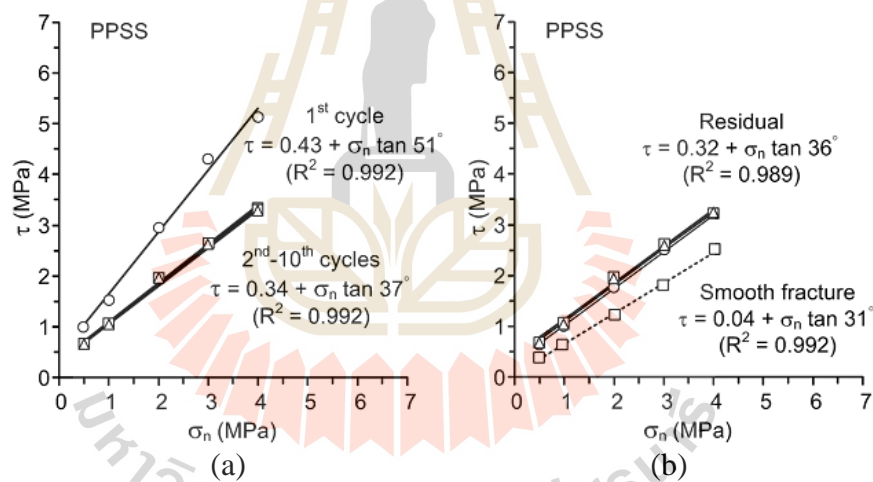


Figure 2.7 Shear strengths (τ) as a function of normal stress (σ_n) for peak (a) and residual (b) (Kamonphet et al., 2015).

Niktabar et al. (2017) study the effect of rock joint roughness on its cyclic shear behavior under cyclic condition were in the present study, regular joints with asperity angles of 15° - 15° and 30° - 30° were prepared. The cyclic shear tests were conducted on regular and irregular joints under different normal stresses are 0.1 MPa,

0.5 MPa and 1 MPa. A total of 30 cycles is made cycles with the shear displacement amplitudes of ± 8 mm. The results obtained indicates that no significant change was observed on the peak shear stress from the first to the last (30th) shear cycle on the joint with 15° - 15° asperity, i.e. the number of shear cycle was not effective on the shear strength. But the shear strength decreased gradually with increasing number of shear cycles for 30° - 30° asperity at normal stress of 0.1 MPa. Mechanism of shearing changed from sliding on the joint with low asperity angle (15° - 15°) to shearing or degradation of asperities on the joint with high asperity angle (30° - 30°) at the same normal stress under cyclic shear loads. With increasing normal stress ($P = 1$ MPa), the peak shear stress increased. But after one or two cycles, the peak shear stress dropped and reached constant values, as demonstrated in Figure 2.8, because all asperities were sheared off after one or two cycles and the mechanism of shearing was the same for both joints. Horizontal displacement corresponding to the peak shear stress decreased with the increase in asperity angle.

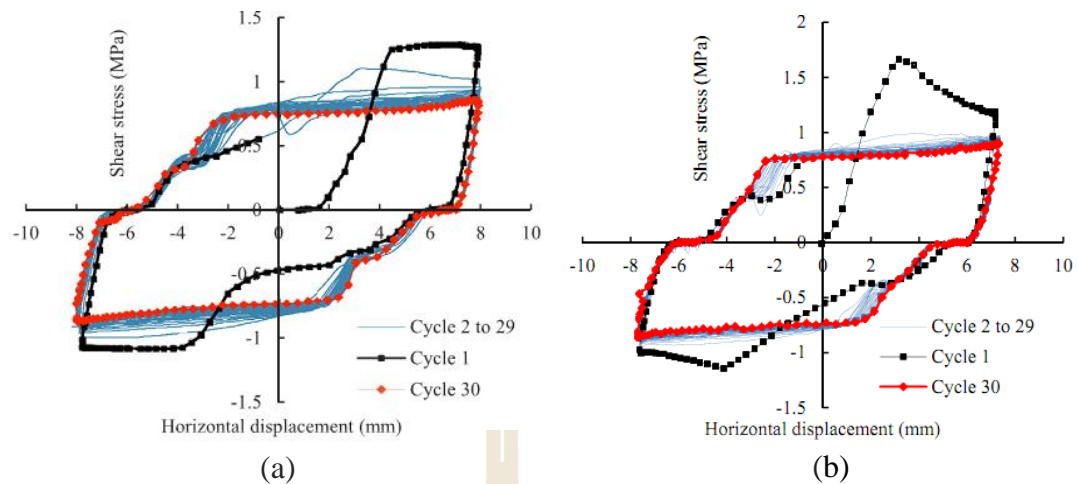


Figure 2.8 Shear stress, normal displacement, and normal stress versus horizontal displacement, respectively, on the joint with 15° - 15° (a) and 30° - 30° (b) asperity angle at normal stresses of 1 MPa (Niktabar et al., 2017).

2.2 Direct shear test

2.2.1 Effects of loading rate on joint shear strength

Chokchai and Fuenkajorn (2013) perform direct shear tests to determine the effects of loading rate on shearing resistance of tension-induced fracture in sandstone specimens. The sandstones are prepared from: Phra Wihan (PW), Phu Phan (PP) and Phu Kradung (PK) formations. The applied shear stresses are controlled at constant rates of 0.00002, 0.0002, 0.002, 0.02 and 0.2 MPa/s. The normal stresses are varied from 0.2, 1, 2, 3 to 4 MPa. The results indicate that for all sandstone types the peak and residual shear strengths and joint shear stiffness increase exponentially with loading rate, particularly under high normal stresses, as shown in Figure 2.9. The shear rate has no effect on the basic friction angle of the smooth saw-cut surfaces. An empirical relation has been developed to represent the shear strengths of the rough fractures under

various loading rates. The results can be used to predict the shear strengths of fractures under various loading rates and normal stresses.

Wang et al. (2016) studies the shear rate on the mechanical behavior of rough rock joints prepared using a molding method by testing jointed samples of four rock joint groups, which were obtained from the underground caverns of the Huangdao State Oil Reserves in China. The tests were performed using a JAW-600 coupled shear-flow machine under constant normal load conditions. Shear rate and joint roughness coefficient (JRC) were the two primary considerations in this study. The results indicate that the peak shear strength is controlled by shear rate and joint roughness. Shear rate has a nonlinear relationship with the peak shear strength, whereas joint roughness exhibits good linearity with a high correlation coefficient (40.97, except for results under a shear rate of 24.0 mm/min). Furthermore, shear rate affects the damage incurred by the rock joints (Figure 2.10).

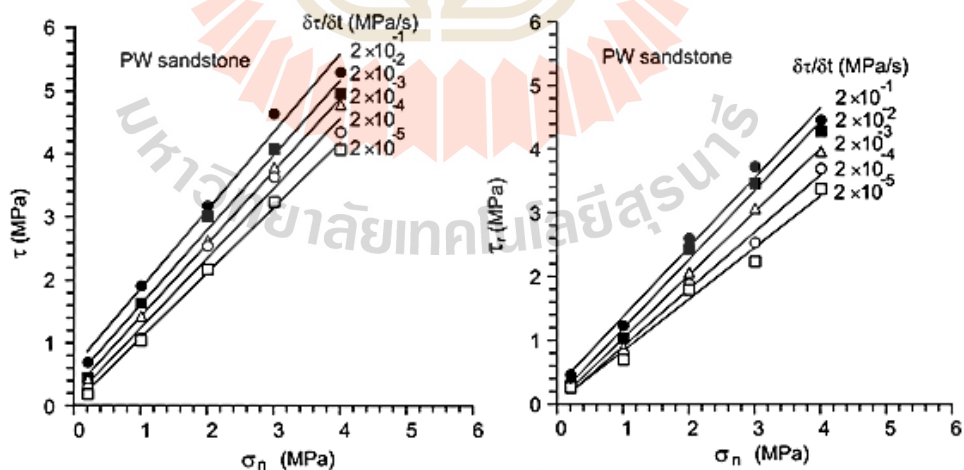


Figure 2.9 Peak (left) and residual (right) shear strengths under various shear rates (Chokchai and Fuenkajorn, 2013).

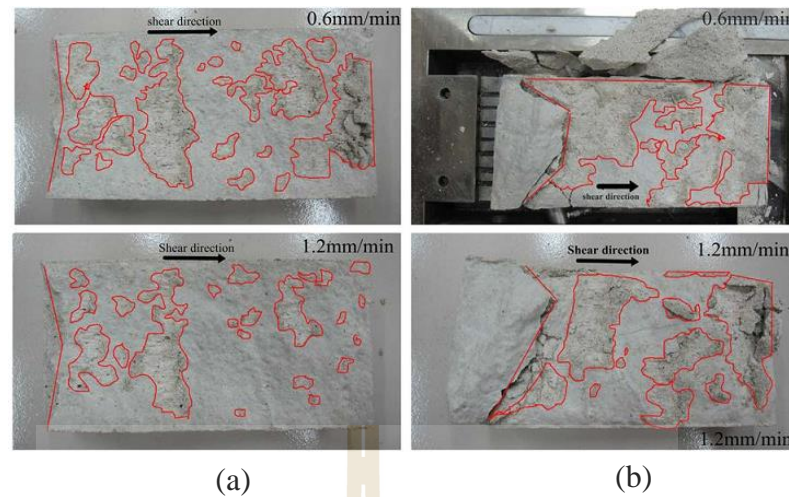


Figure 2.10 Area of damage of the joint surface for groups S3 and S4 sheared under different shear rates: area of damage of the joint surface for group S3 (a); and area of damage of the joint surface for group S4 (b) (Wang et al., 2016).

2.2.2 Effect of rock joint roughness on its shear behavior

Gentier et al. (2000) studies the influence of fracture geometry on shear behavior. Shear tests were performed under applied normal stresses, σ_n , of 7, 14, and 21 MPa. The shear velocity was 0.5 mm/min. Each test was repeated for four different directions (0, -30, 60, 90) denoted by θ (Figure 2.11). The fracture's mechanical response differs depending on the shear direction. The mechanical behavior falls into two categories. The first corresponds to the -30 and 0 directions (parallel to the strike of the fracture), and the second to the 60 and 90 directions (parallel to the dip of the fracture). The results of laboratory experiments on samples with identical fracture geometry show that mechanical parameters depend on shear direction, as shown in Figure 2.12. Gentier et al. (2000) conclude that damaged areas predominated where the local dip direction was close to the shear direction, and also that areas with higher dip values had

the highest probability of damage. The shape of the damage zones depends on the local geometry of the fracture surface, including the size and shape of asperities. The locations of the maximum gradients correspond well to the locations of damage zones for a normal stress of 21 MPa for all shear directions. It must be noted that the damaged areas occurring under normal stresses of 7 MPa and 14 MPa are subsets of the damage zones that result from a normal stress of 21 MPa.

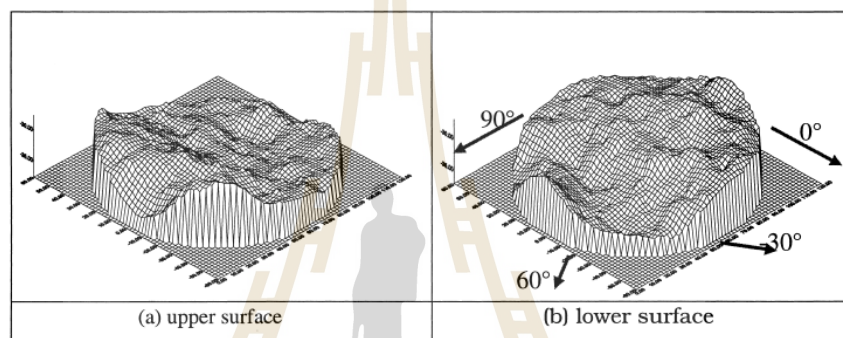


Figure 2.11 Three-dimensional reconstruction of the fracture surfaces (Gentier et al, 2000).

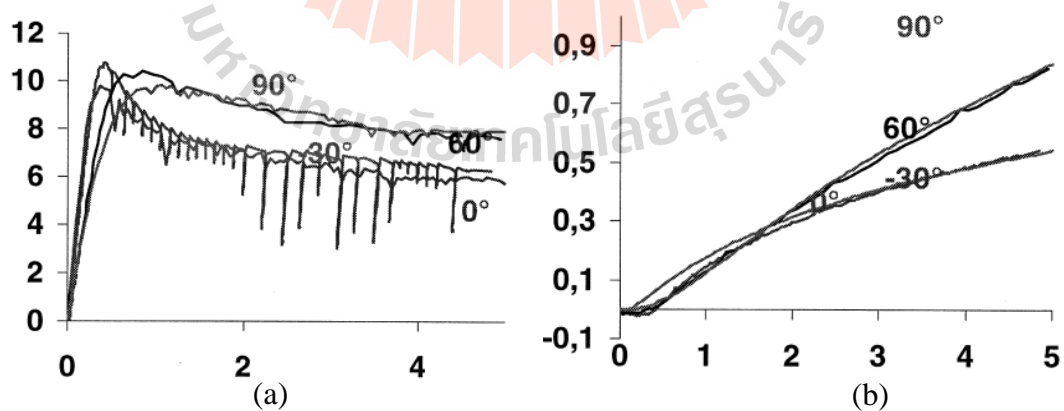


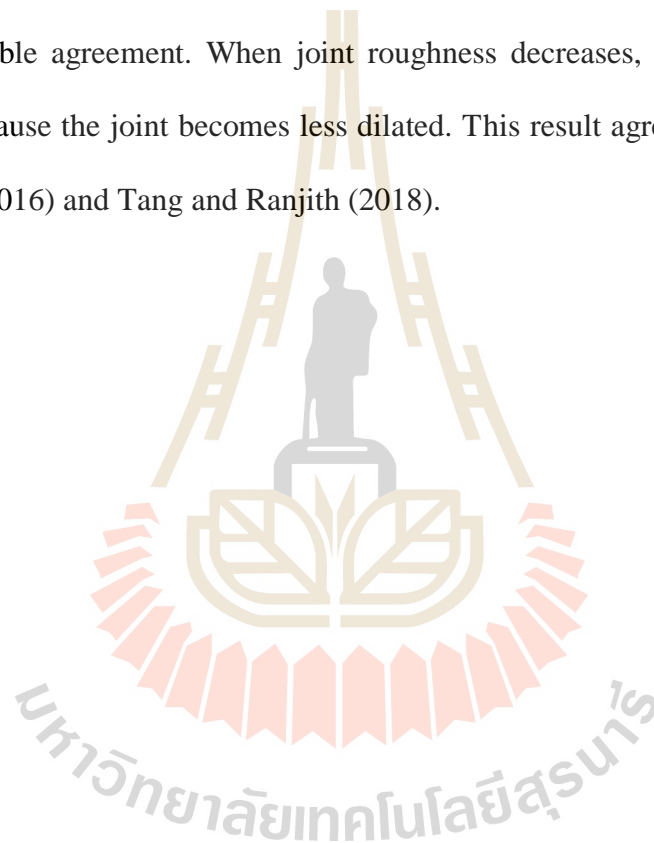
Figure 2.12 Direct shear stress test results: shear stress versus shear displacement (a) and shear stress versus dilatancy in relation to shear direction (b) (Gentier et al, 2000).

Misra (2002) studies the effect of asperity damage on fracture shear behavior. The fracture surface roughness change as a result of asperity damage is modeled by using evolution laws for asperity height and asperity contact orientation distributions. The effect of initial surface roughness upon shear resistance versus shear displacement behavior. The rough fracture has a considerably pronounced softening past peak shear resistance while the smooth fracture exhibits almost no softening behavior. As a result, under higher normal stresses, the asperity damage occurs at a faster rate below peak shear resistance. Consequently, lower peak shear resistance is obtained under higher fracture normal stress, as exemplified in Figure 2.13(a), which gives the peak shear resistance, expressed as friction angle plotted against the fracture normal stress. The corresponding peak shear stress versus fracture normal stress behavior is given in Figure 2.13(b). It is remarkable that the friction angles at higher stresses are considerably lower for a given initial surface roughness. Past peak, in the softening regime, the asperity damage rate is almost same under different normal stresses, therefore, the rate of softening is slower for higher fracture normal stresses.

Fathi et al. (2016) studies the effect of asperities on shear mechanism of rock joints. A series of direct shear tests on coplanar and non-coplanar jointed rocks was simulated using the PFC2D software. The results show that for coplanar jointed rocks, the peak shear stress decreases nonlinearly with the joint persistence, and the failure process can be divided into four stages: elastic shearing phase, crack propagation, failure of rock bridges, and residual phase. For non-coplanar jointed rocks, as the absolute value of the inclination angle of the rock joints increases, its shear strength increases, changing the failure patterns and the length of new fractures between

existing cracks. When the absolute value increases from 15° to 30° , the average shear capacity increases the most as 39%, while the shear capacity increases the least as 2.9% when the absolute value changes from 45° to 60° .

Prasetyo et al. (2017) studies the nonlinear shear behavior of rock joints using a linearized implementation of the Barton-Bandis model. The results show that the general trend of shear behaviors of rock joints for all values of joint length and JRC with reasonable agreement. When joint roughness decreases, less shear strength is obtained because the joint becomes less dilated. This result agrees with Zhao (1997), Johansson (2016) and Tang and Ranjith (2018).



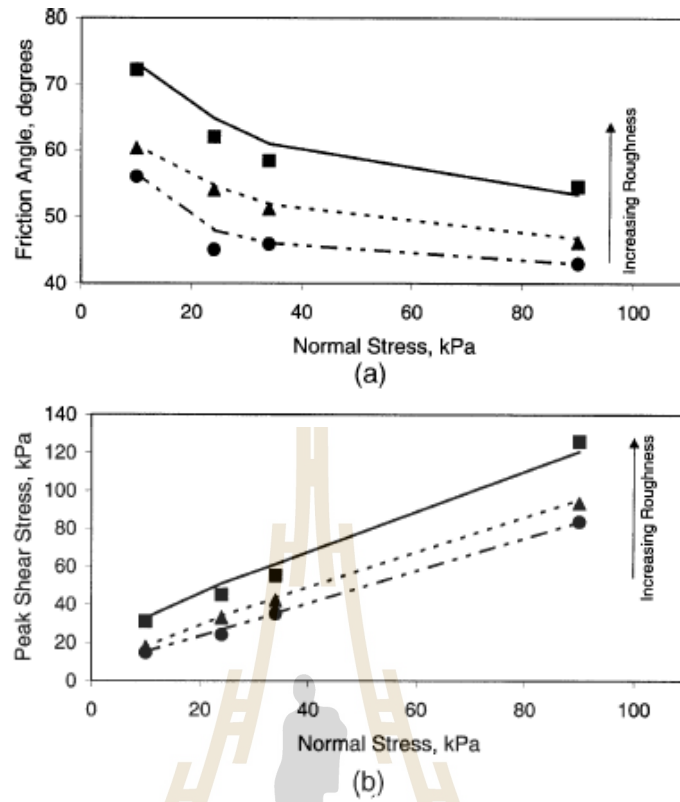


Figure 2.13 Comparison of measured and calculated shear failure behavior of single fractures with different surface roughness: (a) friction angle, and (b) failure envelopes.

CHAPTER III

SAMPLE PREPARATION

3.1 Introduction

This chapter describes the sample preparation and specifications for direct shear tests under cyclic shear loading. The properties the rock samples also identified.

3.2 Sample preparation

The specimens used for the direct shear tests and cyclic shear tests are prepared from Phra Wifhan sandstone. It is fine-grained rock grayish white and composed mainly of quartz and feldspar with a few mica (Kamonphet et al., 2015). They are well sorted and angular. The rock comprises 72% quartz (0.2-0.8 mm), 20% feldspar (0.1-0.8 mm), 3% mica (0.1-0.3 mm), 3% rock fragment (0.5-2 mm), and 2% other (0.5-1 mm) (Khamrat et al., 2016). Figure 3.1 shows the exposure of the Phra Wihan sandstone in the northeast of Thailand. The mechanical properties are shown in Table 3.1. The block specimens are prepared to have nominal dimensions of $10 \times 10 \times 16 \text{ cm}^3$. The fractures have nominal areas of $10 \times 10 \text{ cm}^2$, as shown in Figure 3.2. Specimens with the rough surfaces are prepared by applying a line load at the mid-section of the specimens until splitting tensile failure occurs (tension-induced fractures). Figure 3.3 shows examples of the rock fractures are artificially made in the laboratory by tension inducing method. The asperity amplitudes on the fracture planes are measured from the laser-scanned profiles along the shear direction. The readings are made to the nearest 0.01 mm.

Figure 3.4 shows example of laser scanned images of a tension-induced fracture. The maximum amplitudes are used to estimate the joint roughness coefficients (JRC) of each fracture based on Barton's chart (Barton, 1982). The initial JRC values for the fractures in sandstone is in the ranges of 10 ± 1.0 . Figure 3.5 shows examples of the laser scanned profiles of rock specimens. Table 3.2 shows physical properties of specimens.

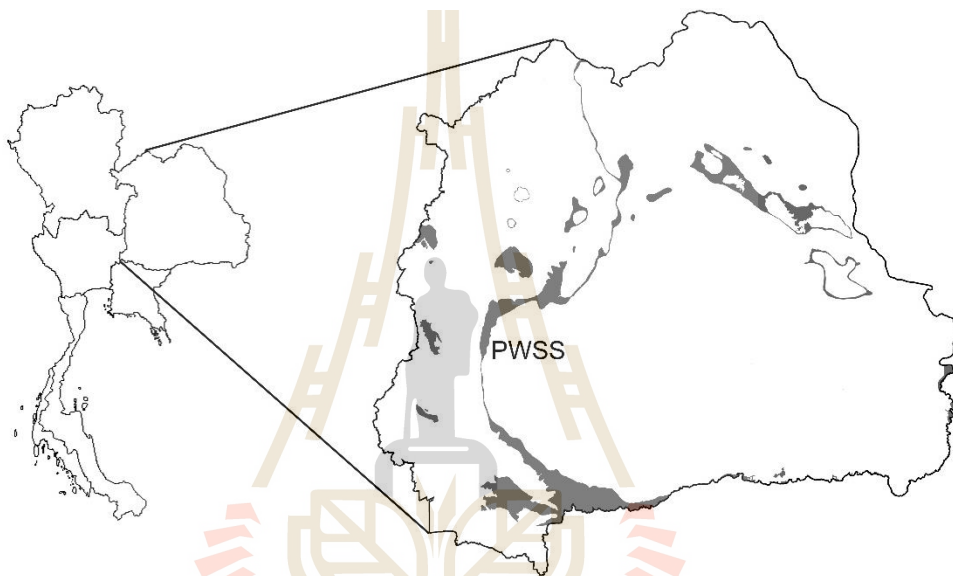


Figure 3.1 Geological map of northeastern Thailand, showing exposure of Phra Wihan sandstone (PWSS) in shade areas.

Table 3.1 Summary of the mechanical properties of rock samples, (Khamrat et al., 2016).

Density (g/cm^3)	Uniaxial Compressive Strength, σ_c (MPa)	Triaxial Compressive Strength	
		Cohesion, c (MPa)	Friction Angle, ϕ (degrees)
2.25 ± 0.06	41.0 ± 11.0	9.1	42

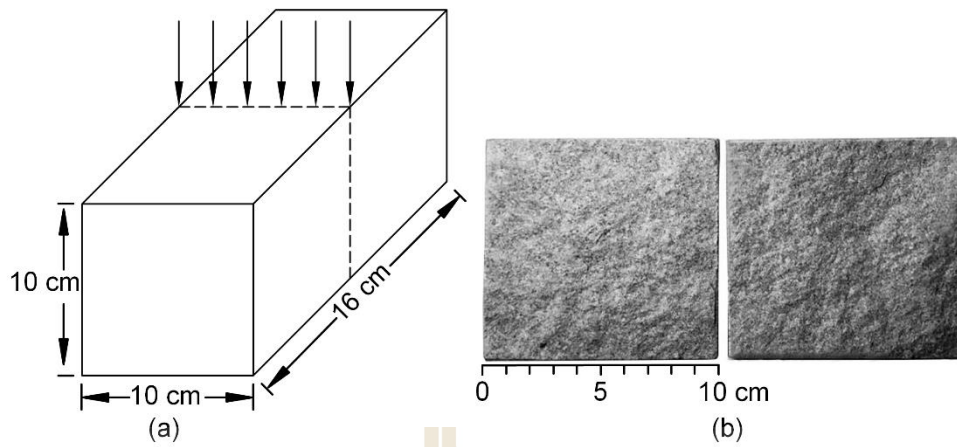


Figure 3.2 Line load applied at the mid-section of the specimens to obtain a tension-induced fractures (a), and example of tension-induced fractures (b).

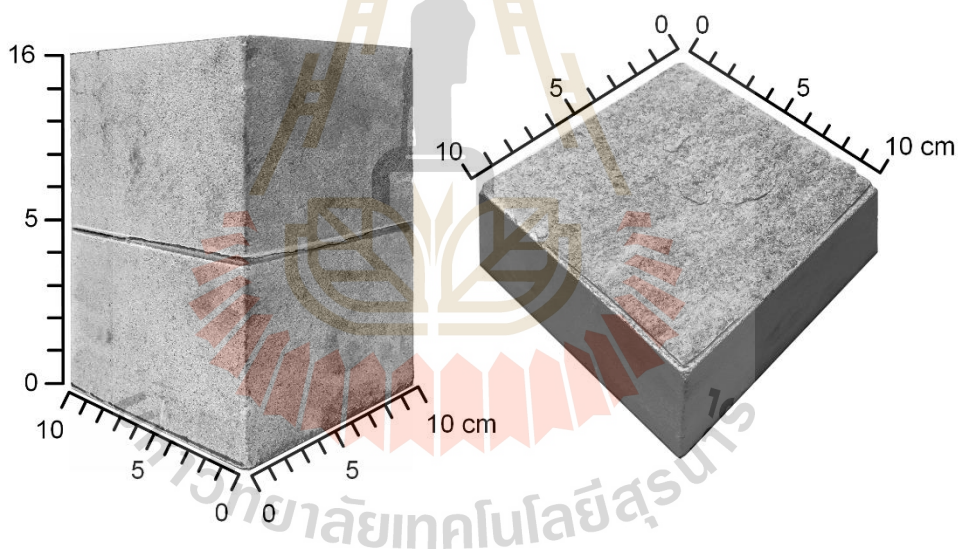


Figure 3.3 Examples of the rock fracture.

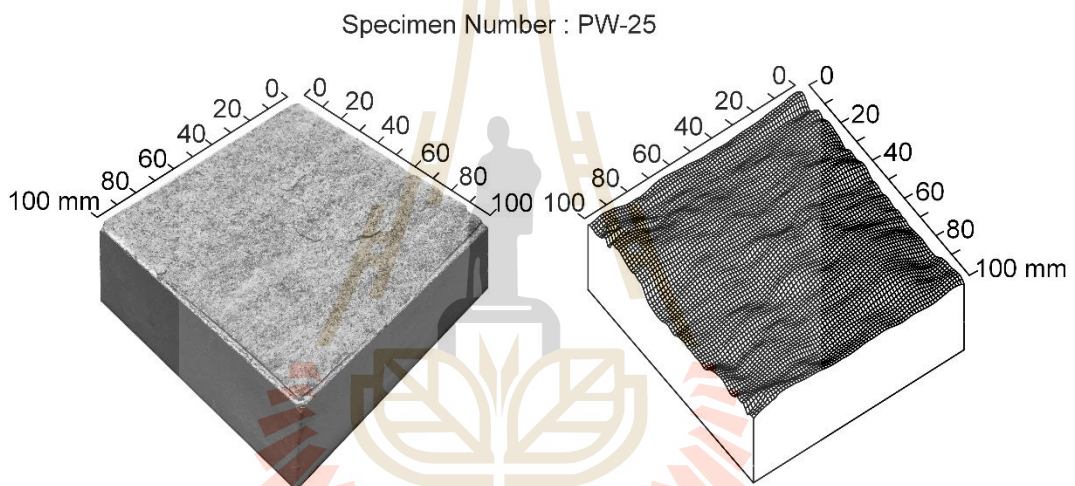
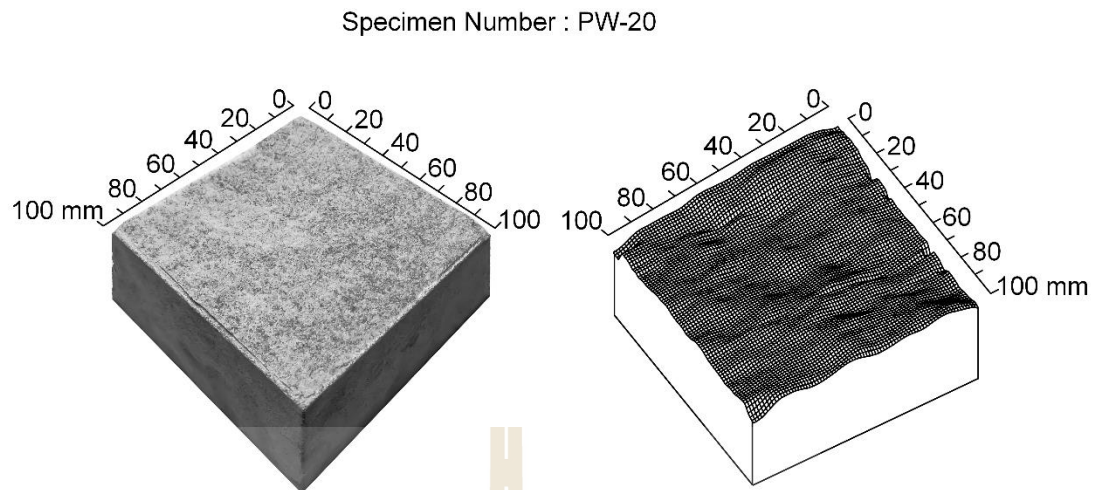


Figure 3.4 Some tension-induced fractures and their laser scanned images.

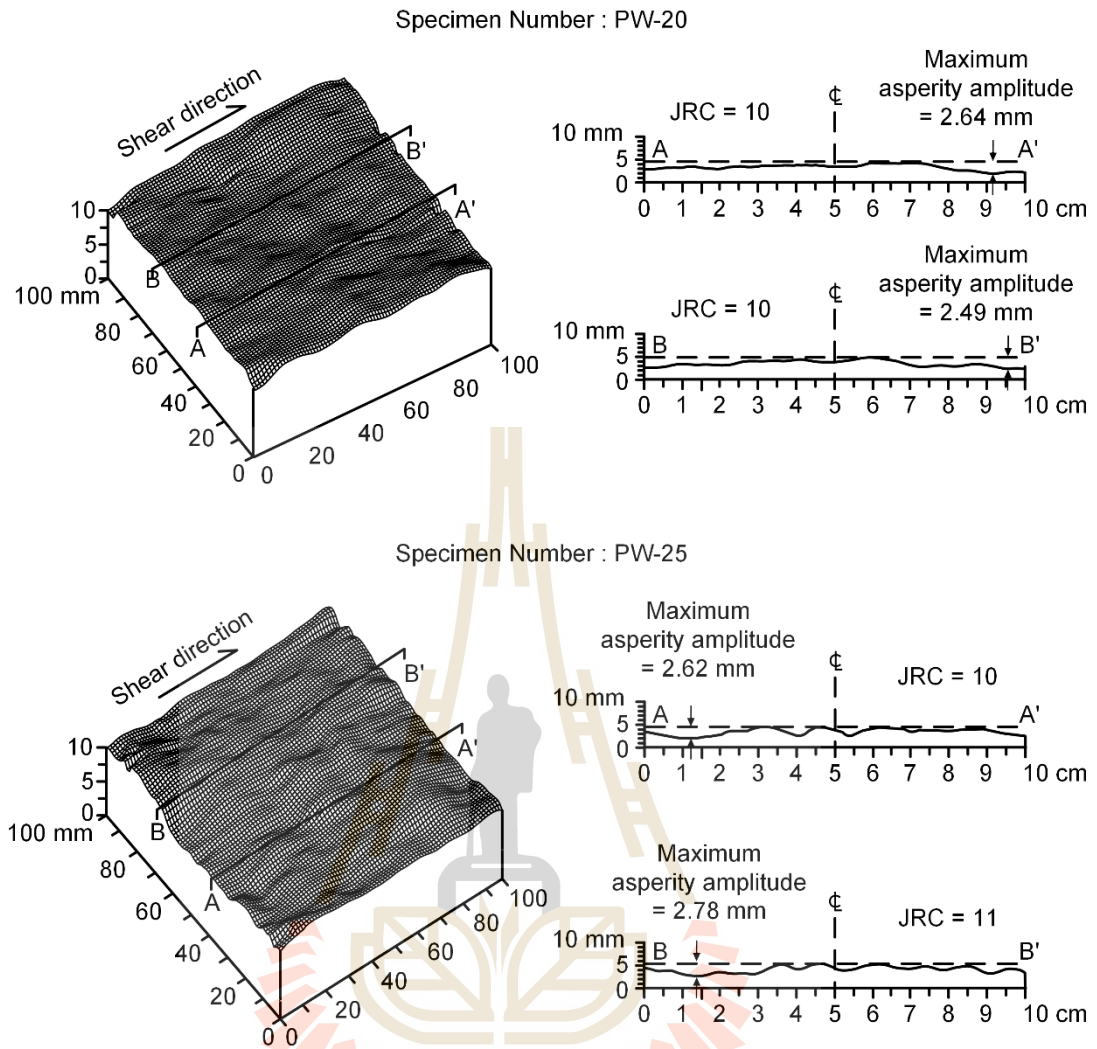


Figure 3.5 Examples of laser-scanned profiles used to measure the maximum asperity amplitude to estimate the joint roughness coefficient (JRC).

Table 3.2 Summary of sample dimensions and their fracture roughness (JRC).

Specimen No.	Dimension (mm³)	Density (g/cc)	JRC
PW-01	101.5×102.0×181.7	2.31	10
PW-02	101.6×101.8×182.2	2.30	10
PW-03	102.0×102.9×182.2	2.30	10
PW-04	101.5×100.6×182.3	2.30	10
PW-05	102.5×102.3×182.5	2.32	10
PW-06	102.3×102.2×183.0	2.28	10
PW-07	101.1×102.4×182.4	2.30	10
PW-08	102.5×104.2×182.8	2.34	10
PW-09	101.7×102.3×182.2	2.32	10
PW-10	103.8×102.4×182.4	2.33	10
PW-11	101.7×101.7×181.6	2.29	10
PW-12	101.9×102.1×181.7	2.30	10
PW-13	103.1×105.2×182.1	2.25	10
PW-14	103.0×102.0×181.9	2.33	11
PW-15	101.6×102.7×182.5	2.40	10
PW-16	101.7×103.7×183.8	2.29	10
PW-17	101.7×101.3×182.2	2.35	10
PW-18	101.3×102.5×181.7	2.33	10
PW-19	101.1×100.0×182.0	2.37	10
PW-20	102.3×104.7×182.8	2.32	10
PW-21	103.2×102.2×182.2	2.34	10
PW-22	102.2×101.5×182.1	2.33	10
PW-23	102.3×101.8×182.0	2.32	10
PW-24	102.6×102.6×182.0	2.30	10
PW-25	102.8×102.6×181.6	2.32	11
PW-26	101.7×102.4×181.7	2.32	10
PW-27	101.1×102.6×182.7	2.32	11
PW-28	100.9×102.4×181.8	2.31	10
PW-29	102.8×100.9×181.9	2.34	10
PW-30	102.6×100.9×182.7	2.32	10
PW-31	100.9×102.5×182.6	2.31	10
PW-32	101.9×101.7×182.0	2.30	10
PW-33	101.8×102.8×182.6	2.32	10
PW-34	100.6×102.0×182.2	2.31	10
PW-35	104.0×103.0×182.5	2.31	10
PW-36	101.6×102.5×182.8	2.36	10

CHAPTER IV

LABORATORY TEST

4.1 Introduction

The objective of this section is to describe the apparatus and method to determine the shear resistance of fractures under monotonic cyclic loading. The laboratory tests are divided into three series; 1) direct shear test, 2) cyclic shear test under constant shear stress amplitude and 3) cyclic shear test under constant shear displacement amplitude.

4.2 Direct shear test

The test method and calculation for the direct shear test follow the ASTM (D5607-08) standard and the ISRM suggested method (Brown, 1981). Each specimen is sheared once under each normal stress using a direct shear device (SBEL DR44, capacity of 10,000 pounds normal load and 30,000 pounds shear force) (Figure 4.1). The applied constant normal stresses are 1, 2, 3 and 4 MPa. The shear rate is maintained constant at 0.01-0.02 mm/s. Shear force is continuously applied until a total shear displacement of 5 mm is reached. The displacement dial gages used to measure the shear displacement and fracture dilation. The direct shear test is determined peak and residual joint shear strength. The shear strength (τ) is calculated by equation;

$$\tau = P/A \tag{4.1}$$

where P is the shear force and A is the contact area between both specimens. The test results are shown in forms of the shear strength as a function of normal stress. The peak shear strength is used to calculate the cohesion and friction angle.

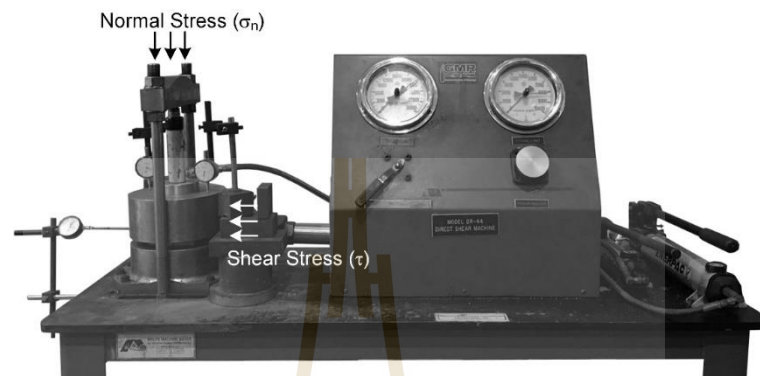
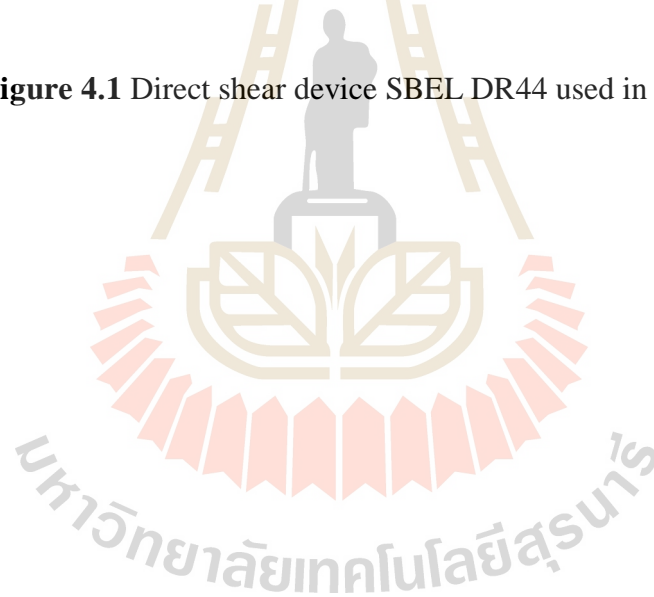


Figure 4.1 Direct shear device SBEL DR44 used in this study.



4.3 Cyclic shear test under constant shear stress amplitude

The cyclic shear test under constant shear stress amplitude applied constant normal stresses are 1, 2, 3 and 4 MPa. The shear rate is maintained constant at 1 kN/s. A total of 50 cycles is made cycles with the shear stress amplitudes of 25, 50 and 75% of the peak shear strength. The dial gages measure the shear and normal displacements. The loading cycle in forward-backward cyclic shear testing each loading cycle are divided into four stages: forward advance (stage I) to reach the defined maximum stress; return (stage II) to decrease the shear stress to 0 MPa; backward advance (stage III) to reversely increase to the maximum stress; backward return (stage IV) to decrease from the shear stress to 0 MPa (Figure 4.2). The cyclic shear loading shear stress amplitude results are presented in forms of the shear strength as a function of shear displacement. After the cyclic loading test is completed for 50 cycles, the sheared fractures are again subjected to monotonic loading beyond the peak strength to assess the effect of cyclic loading on the peak and residual strengths of the fractures.

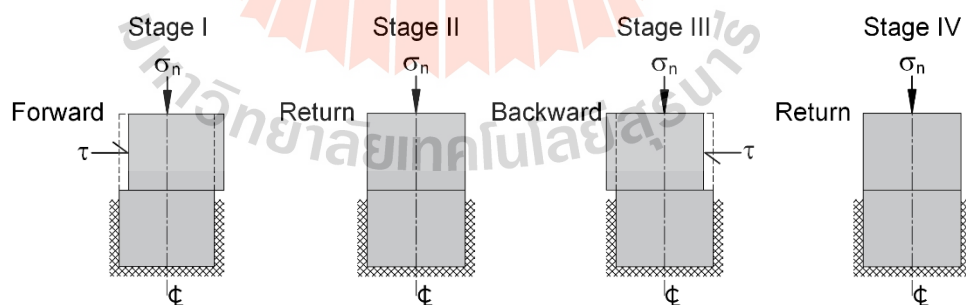


Figure 4.2 Shearing path for constant shear stress amplitude in one cycle.

4.4 Cyclic shear test under constant shear displacement amplitude

The cyclic shear test under constant shear displacement amplitude applied constant normal stresses are 1, 2, 3 and 4 MPa. The shear displacement rate are maintained constant at 0.01-0.02 mm/sd. A total of 50 cycles is made cycles with the shear displacement amplitude of 25, 50 and 75% of the peak shear displacement. The dial gages measure the shear and normal displacements. The loading cycle in forward-backward cyclic shear testing each loading cycle is divided into four stages: forward advance (stage I) to reach the defined maximum shear displacement; return (stage II) to decrease the shear displacement to 0 mm; backward advance (stage III) to reversely increase to the maximum shear displacement; backward return (stage IV) to decrease from the shear displacement to 0 mm (Figure 4.3). The cyclic shear loading shear displacement amplitude results are shown in forms of the shear strength as a function of shear displacement. After the cyclic loading test is completed for 50 cycles, the sheared fractures are again subjected to monotonic loading.

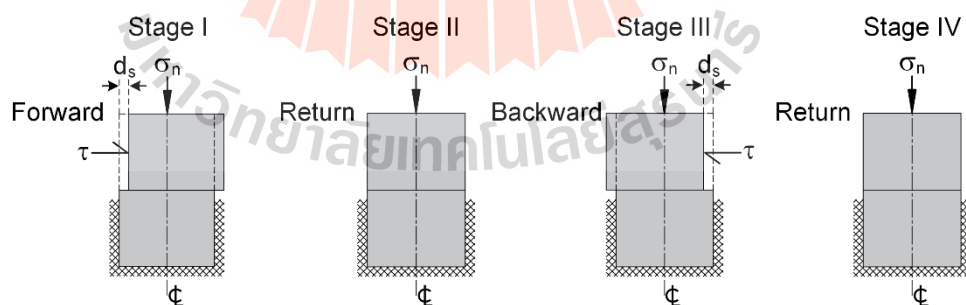


Figure 4.3 Shearing path for constant shear displacement amplitude in one cycle.

CHAPTER V

TEST RESULTS

5.1 Introduction

Three test series are performed as follows: 1) direct shear test, 2) cyclic shear test under constant shear stress amplitude, and 3) cyclic shear test under constant shear displacement amplitude. This chapter describes the test results.

5.2 Direct shear test

The monotonic loading direct shear results are presented in terms of the shear stresses as a function of shear displacement for each normal stress with a constant shearing rate of 0.01-0.02 mm/s. The test method and calculation are in accordance with the ASTM (D56077-08) standard practice. Figure 5.1 shows shear stress-displacement curves under 1, 2, 3 and 4 MPa normal stresses. It is clearly that the shear strengths increase with increasing the normal stresses. The cohesion and friction angle of the fractures under peak strength equal to 0.9 MPa and 40 degrees (Figure 5.2). The peak strengths and displacements are used to define the shear stress and shear displacement amplitudes for the subsequent cyclic shear testing under constant stress and constant displacement conditions, as shown in Table 1. Post-test observations of the sheared fractures suggest that the higher normal stresses are applied, the larger sheared-off areas are obtained, as shown in Figure 5.3.

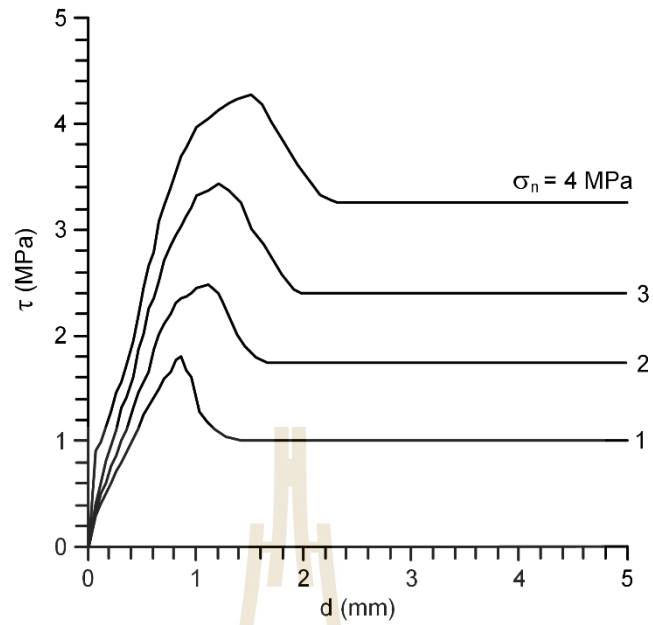


Figure 5.1 Shear stresses as a function of shear displacement.

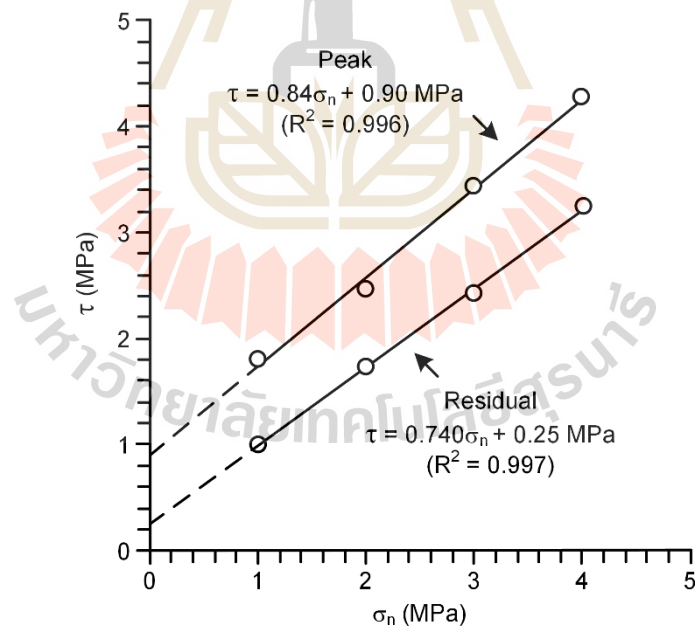


Figure 5.2 Peak and residual shear strength as a function of normal stress.

Table 5.1 Test variables for constant shear stress amplitude and constant shear displacement amplitude.

σ_n (MPa)	Monotonic loading		Cyclic loading	
	τ_p (MPa)	d_p (mm)	Constant shear stress amplitude (MPa)	Constant shear displacement amplitude (mm)
1	1.80	0.85	0.50 (0.25 τ_p)	0.23 (0.25 d_p)
			1.00 (0.50 τ_p)	0.45 (0.50 d_p)
			1.40 (0.75 τ_p)	0.68 (0.75 d_p)
2	2.47	1.10	0.60 (0.25 τ_p)	0.28 (0.25 d_p)
			1.20 (0.50 τ_p)	0.55 (0.50 d_p)
			1.80 (0.75 τ_p)	0.83 (0.75 d_p)
3	3.43	1.20	0.85 (0.25 τ_p)	0.30 (0.25 d_p)
			1.70 (0.50 τ_p)	0.60 (0.50 d_p)
			2.55 (0.75 τ_p)	0.90 (0.75 d_p)
4	4.27	1.50	1.20 (0.25 τ_p)	0.38 (0.25 d_p)
			3.00 (0.50 τ_p)	0.75 (0.50 d_p)
			3.50 (0.75 τ_p)	1.13 (0.75 d_p)

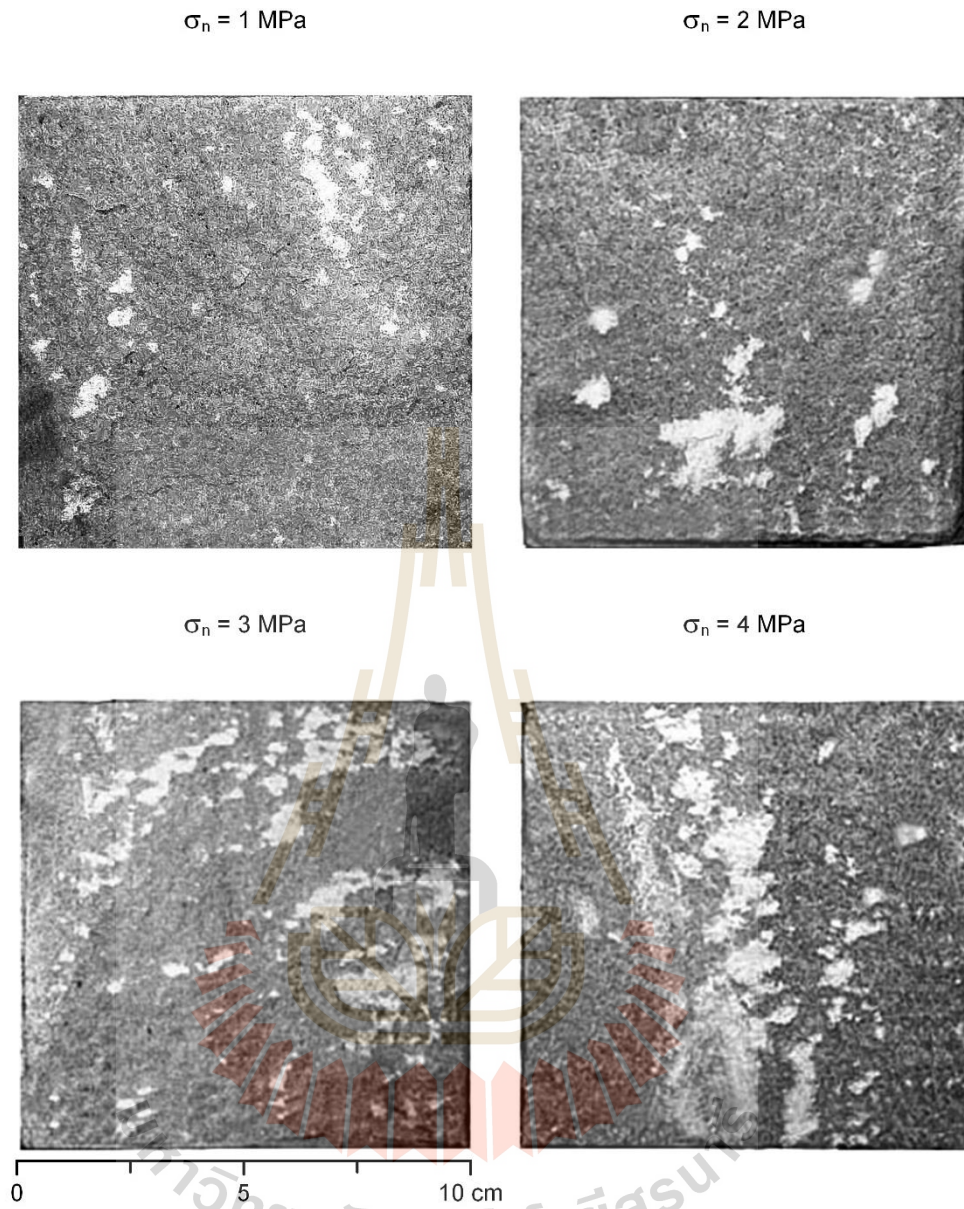


Figure 5.3 Post-test fractures under conventional monotonic shear testing.

5.3 Cyclic test under constant shear stress amplitude

Figure 5.4 shows shear stress (τ) as a function of shear displacement (d) under constant shear stress amplitude with normal stresses of 1, 2, 3 and 4 MPa. All specimens show that the shear displacement for each cycle increases with increasing shear cycles, particularly under high shear stress amplitude (τ_A). After the first few cycles under high stress amplitude ($\tau_A = 1.4$ MPa or 75% of peak strength, τ_P), the shear displacement progresses in the forward direction more than that in the backward direction. This may be due to that the sheared-off rock powder has deposited in the fracture aperture. The larger number of shear cycles, the more rock powder has deposited in the aperture. This phenomenon has not been observed for the lower stress amplitude ($\tau_A = 0.5$ MPa or 25% of peak strength) testing. The results also suggest that the cyclic loading with shear stress amplitudes from 25% to 75% of the peak strength has some impact on the fracture shear strength.

Figure 5.5 shows the fracture shear stiffness (K_s) as a function of number of cycles (N) under constant normal stresses of 1, 2, 3 and 4 MPa. The results indicate that the shear stiffness rapidly decreases within the first few cycles. This is probably due to the degradation of the second order fracture asperities. The fracture stiffness tends to approach a certain value after 50 shear cycles.

Figure 5.6 plots the post-test JRC's as a function of shear stress amplitude (0.25, 0.5 and $0.75\tau_P$). The results show that the JRC decreases with the increase of normal stresses and shear cycles. Figure 5.7 shows the post-test fractures after 50 shear cycles, suggesting that the higher shear stress amplitude ($\tau_A = 3.5$ MPa or 75% of peak strength) and normal stress ($\sigma_n = 4$ MPa) are applied, the larger sheared-off areas are obtained. The sheared-off areas are the results of the degradation of the second order asperities.

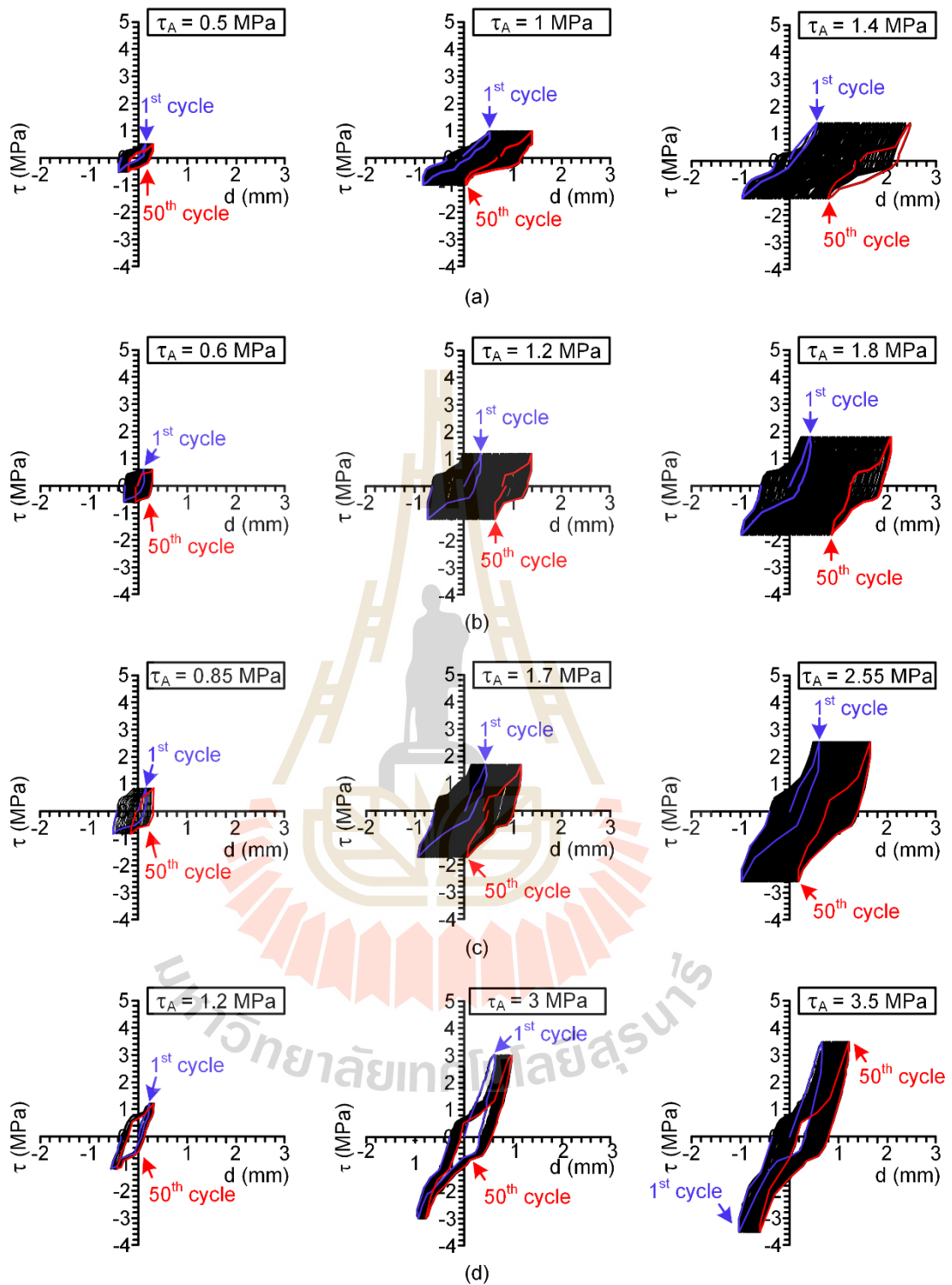


Figure 5.4 Shear stress-displacement curves for constant shear stress amplitude under normal stresses of 1 MPa (a), 2 MPa (b), 3 MPa (c) and 4 MPa (d).

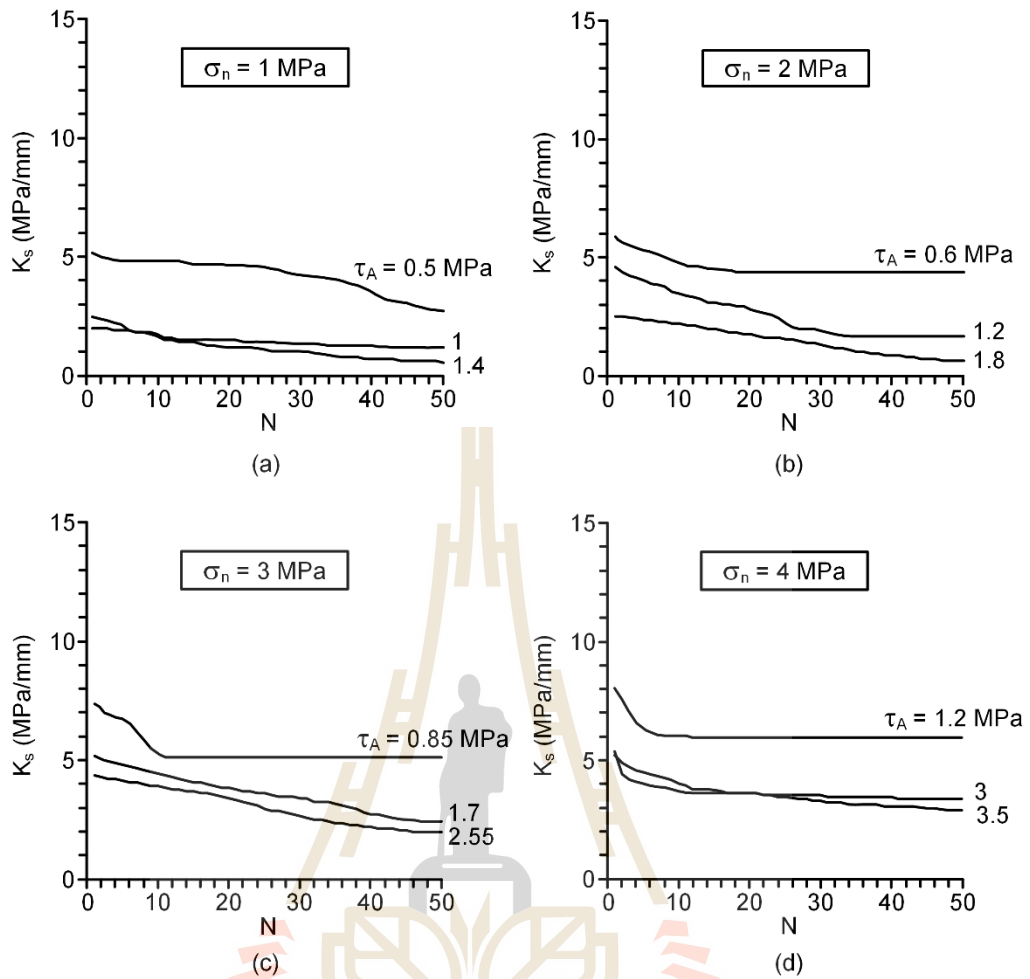


Figure 5.5 Fracture shear stiffness (K_s) as a function of shear cycle (N) under normal stresses of 1 MPa (a), 2 MPa (b), 3 MPa (c) and 4 MPa (d).

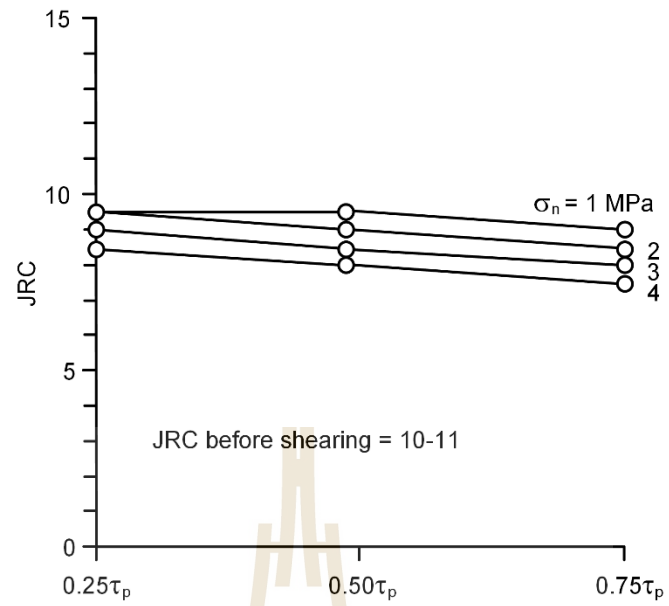
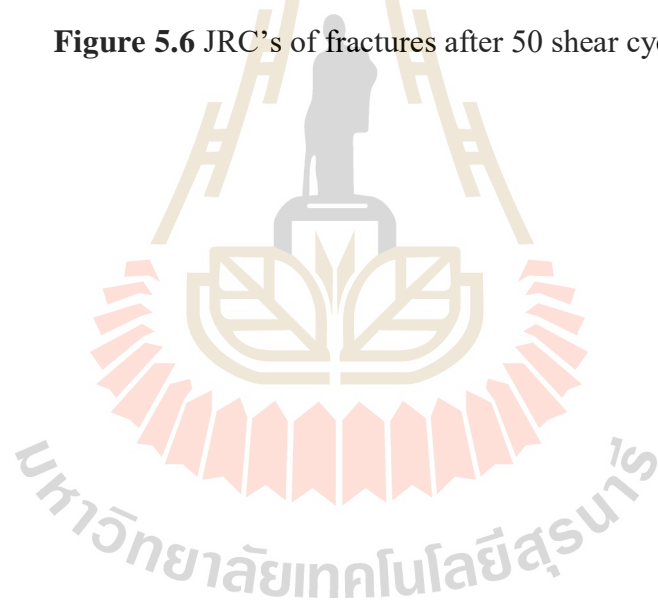


Figure 5.6 JRC's of fractures after 50 shear cycles.



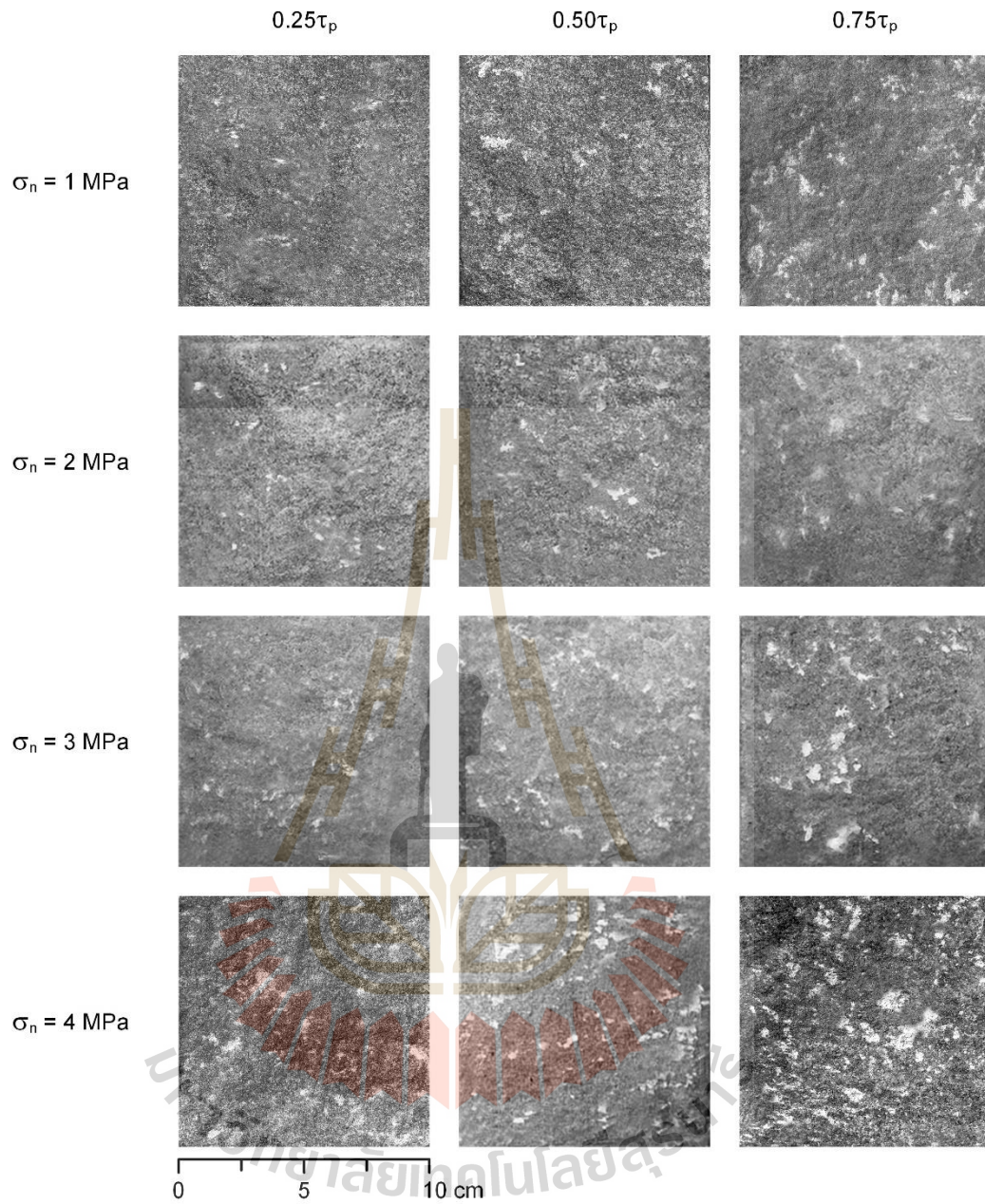


Figure 5.7 Post-test fractures after 50 shear cycles.

5.4 Cyclic test under constant shear displacement amplitude

Figure 5.8 shows the cyclic loading results under constant shear displacement amplitude (d_A). The shear stress of each cycle decreases with increasing loading cycles, particularly under high normal stress and large displacement amplitude ($d_A = 1.13$ mm or 75% of d_p). This may be because the second order asperities have been sheared-off during the first few loading cycles. Smaller shear stresses are therefore required for the subsequent cycles to reach the same displacement amplitude (d_A). This observation holds true for all normal stresses and all displacement amplitudes. Similar to the constant stress amplitude testing, the pre-peak cyclic loading under constant displacement amplitudes (d_A) also has some impact on the fracture shear strengths. Figure 5.9 shows the fracture shear stiffness (K_s) as a function of number of cycles (N) under constant normal stresses of 1, 2, 3 and 4 MPa. The results indicate that the fracture shear stiffness decreases within the first few cycles. This is probably due to the degradation of the second order fracture asperities. The stiffness tends to approach certain values after 10 to 20 loading cycles (N).

Figure 5.10 plots the post-test JRC's as a function of shear displacement amplitude (0.25, 0.5 and 0.75 d_p). The JRC decreases with the increasing normal stresses and shear cycles. Figure 5.11 shows the post-test fractures of the cyclic shear test under constant shear displacement amplitude. In the figure the light areas represent the sheared-off areas with slight amount of rock powder deposition. The sheared-off areas increases with increasing shear displacement amplitude and normal stress.

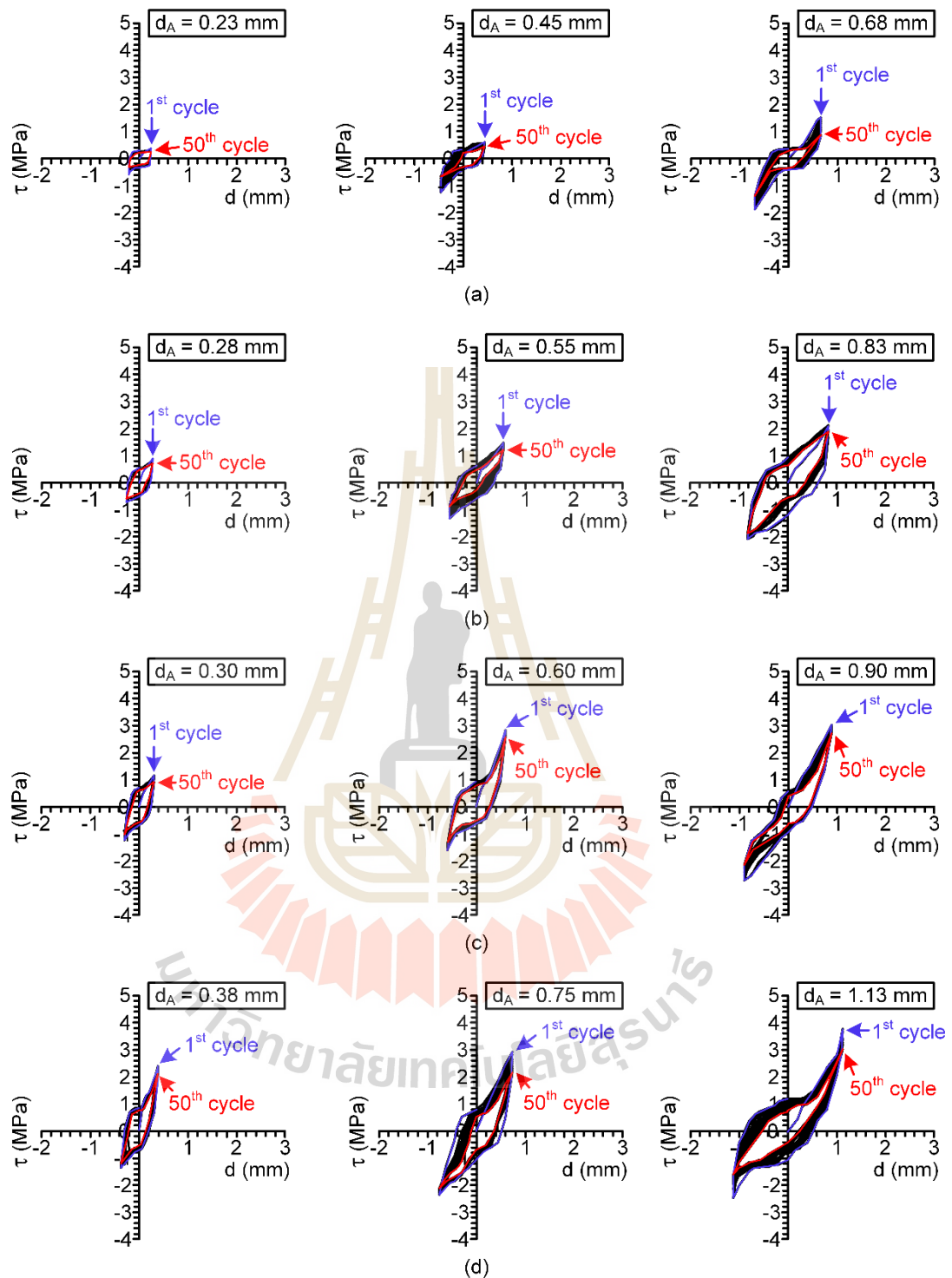


Figure 5.8 Shear stress-displacement curves for constant shear displacement amplitude under normal stresses of 1 MPa (a), 2 MPa (b), 3 MPa (c) and 4 MPa (d).

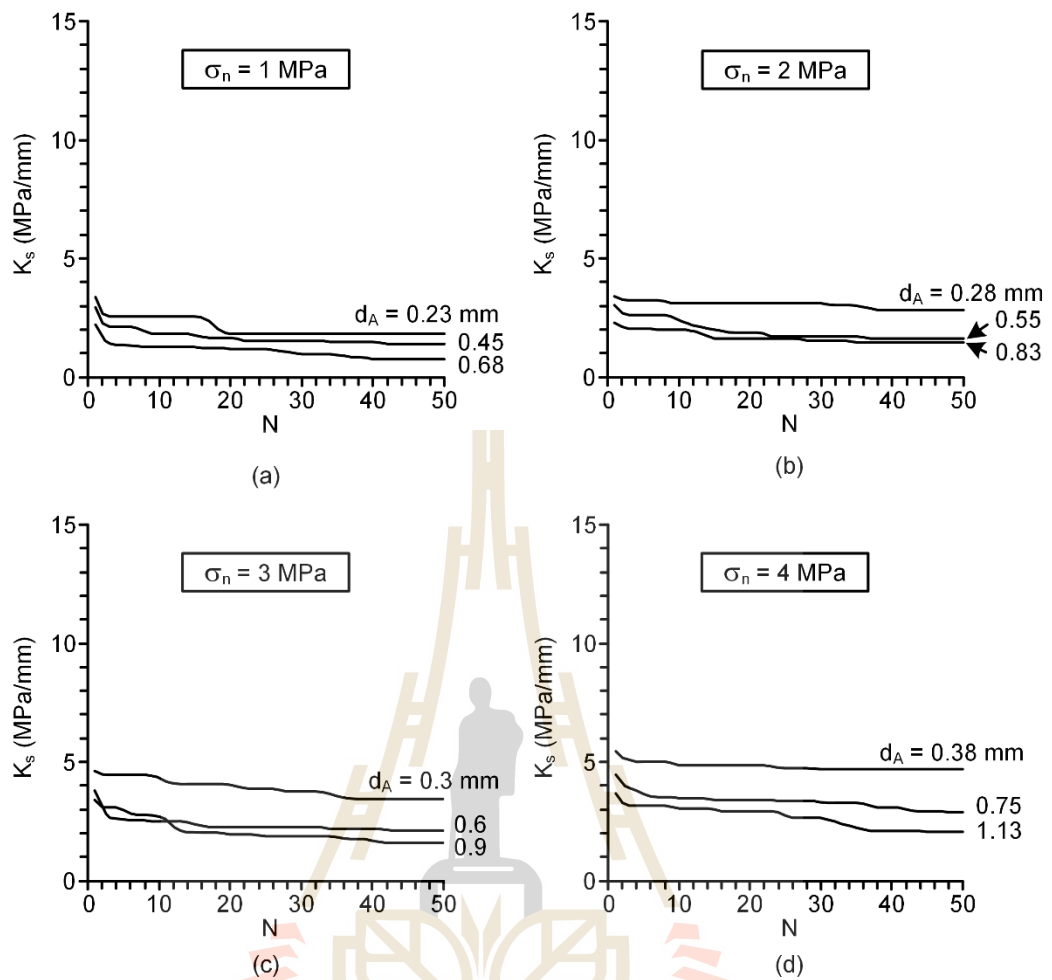


Figure 5.9 Fracture shear stiffness (K_s) as a function of shear cycle (N) under normal stresses of 1 MPa (a), 2 MPa (b), 3 MPa (c) and 4 MPa (d).

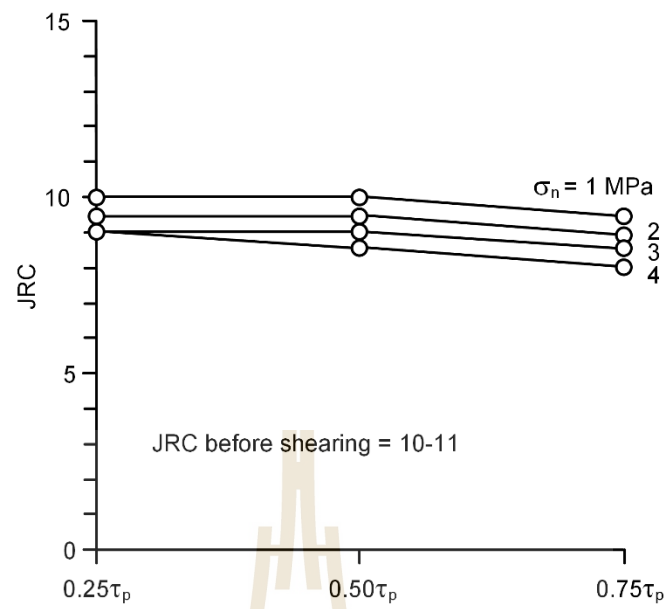
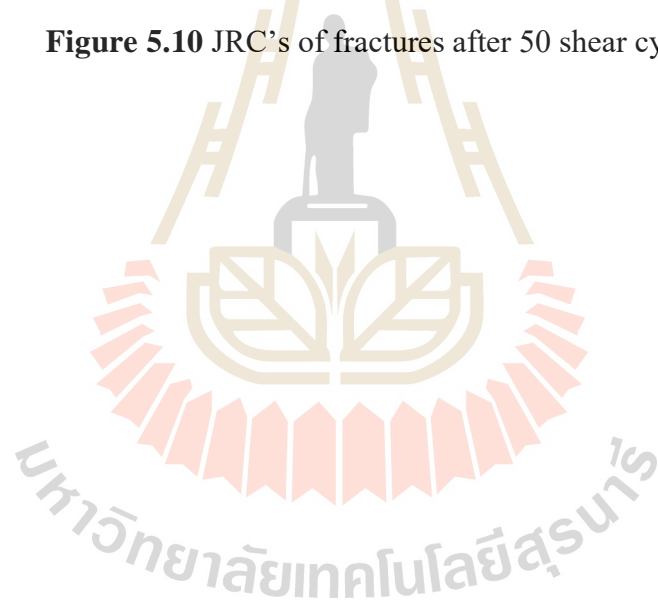


Figure 5.10 JRC's of fractures after 50 shear cycles.



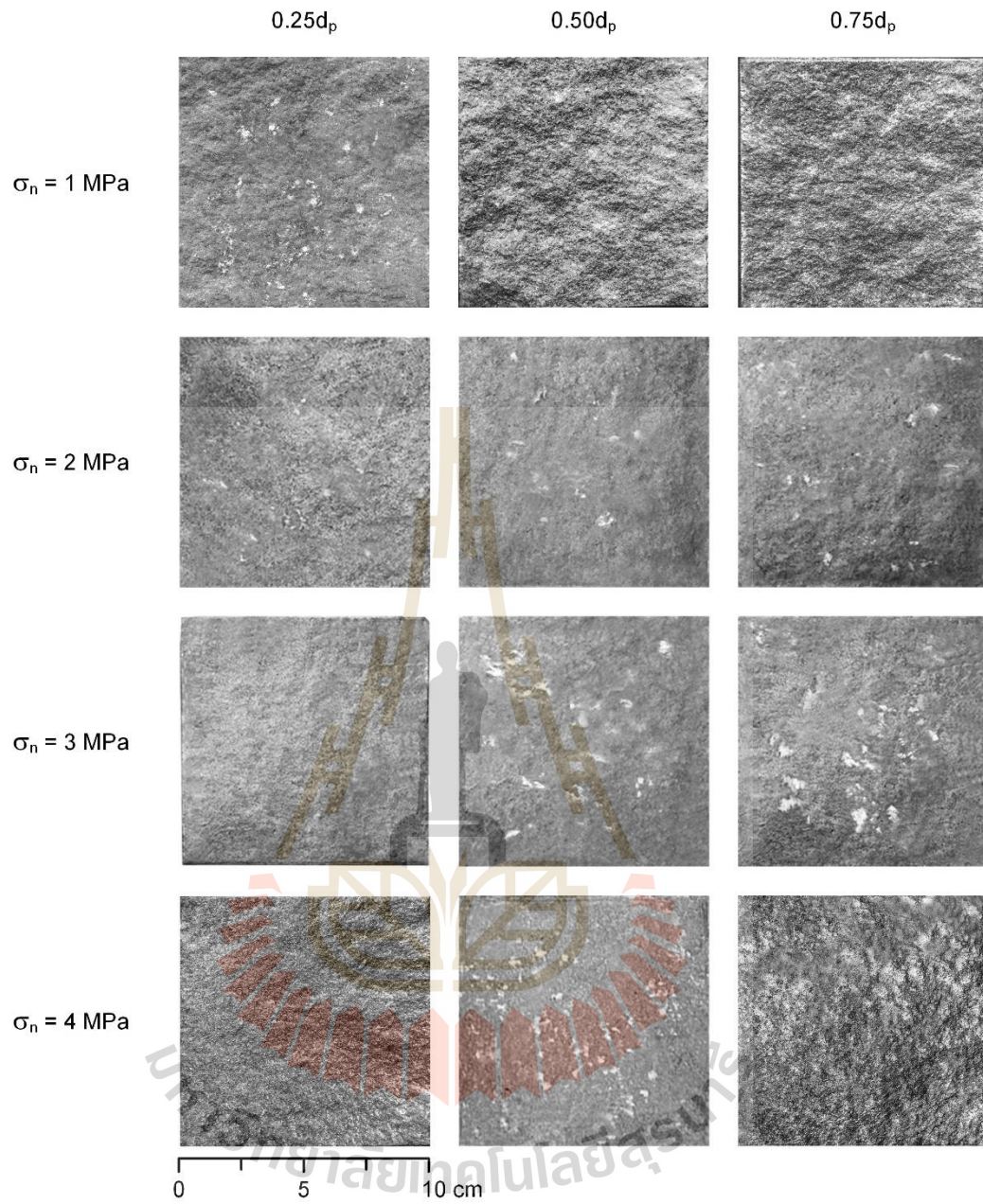


Figure 5.11 Post-test fractures after 50 shear cycles.

5.5 Monotonic direct shear test after cyclic loading

Figure 5.12 shows shear stress (τ) as a function of normal stress for constant shear stress amplitude (Figure 5.12a) and constant shear displacement amplitude (Figure 5.12b). The results show that the shear strength of under monotonic loading of identical fractures (no cyclic loading, solid lines in Figure 5.12) are slightly higher than those of the fractures after subjecting to the cyclic loading (dash line in Figure 5.12). Table 5.2 shows peak shear strength after 50 cycles for constant stress and constant displacement amplitudes. Table 5.3 shows that the friction angle and cohesion decrease with increasing shear stress and displacement amplitudes. The monotonic loading of the identical fracture is slightly higher than those of the fractures after subjecting to the cyclic loading.

The fracture shear stiffness (K_s) values for both cyclic test conditions are determined and compared with those of the monotonic loading on the original fractures and on the fractures after subjecting to cyclic loading. The results are shown in Figure 5.13 and Figure 5.14 for normal stresses of 1, 2, 3 and 4 MPa. Both cyclic loading tests show rapid decreases of K_s within the first few cycles due to the degradation of the second order fracture asperities. Fractures under constant stress amplitudes (Figure 5.13) tend to degrade more quickly than those under constant displacement amplitude (Figure 5.14). The fracture shear stiffness under monotonic loading ($K_{s,post}$) after subjecting to cyclic loading is slightly lower than that of the original fractures ($K_{s,pre}$). This supports the previous observations that the shear strengths of the original fractures are slightly higher than those of the fractures after subjecting to cyclic loading.

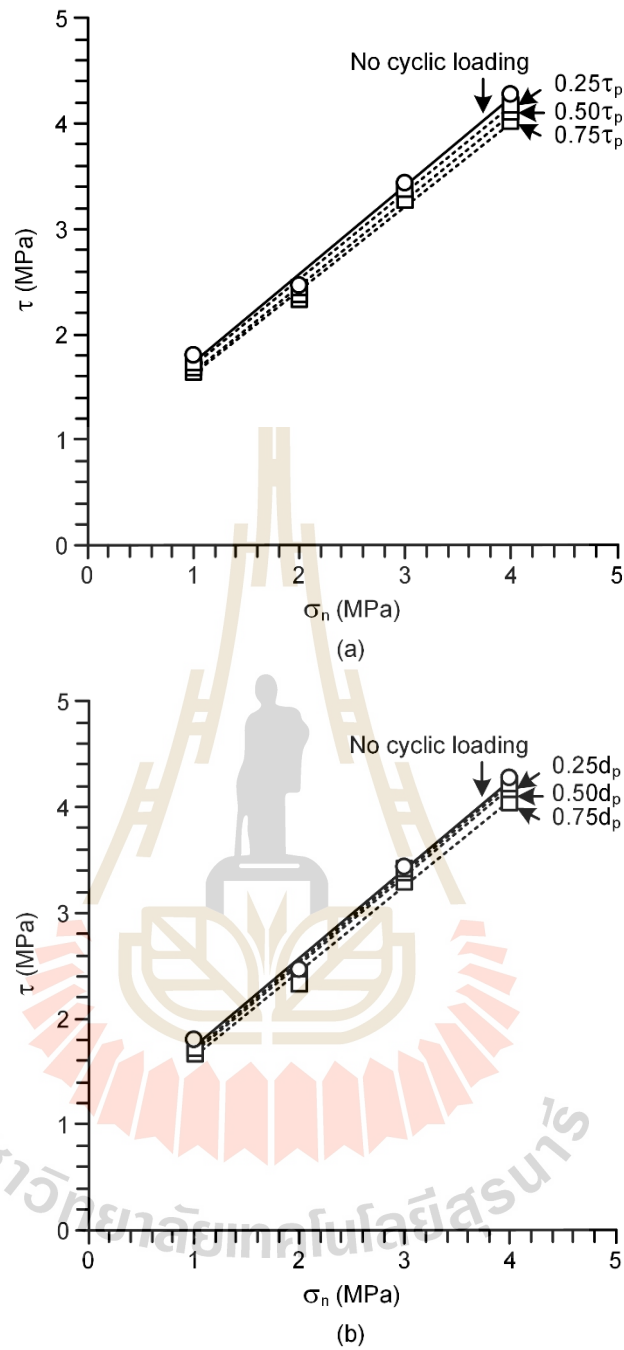


Figure 5.12 Peak shear strengths as a function of normal stress cycles for constant stress amplitudes (a) and constant displacement amplitude (b). Solid and dash lines are monotonic loading of original fractures and of fractures after cyclic loading, respectively.

Table 5.2 Peak shear strength after 50 cycle for constant shear stress amplitude and constant shear displacement amplitude.

Monotonic loading		Cyclic loading					
		Constant shear stress amplitude (MPa)			Constant shear displacement amplitude (MPa)		
σ_n (MPa)	τ_p (MPa)	$0.25\tau_p$	$0.50\tau_p$	$0.75\tau_p$	$0.25d_p$	$0.50d_p$	$0.75d_p$
1	1.80	1.75	1.69	1.67	1.76	1.74	1.69
2	2.47	2.44	2.40	2.34	2.44	2.41	2.36
3	3.43	3.40	3.36	3.29	3.44	3.41	3.31
4	4.27	4.18	4.10	4.03	4.22	4.19	4.06

Table 5.3 Friction angle and cohesion after 50 cycle for constant shear stress amplitude and constant shear displacement amplitude.

Parameter	Monotonic loading	Cyclic loading					
		Constant shear stress amplitude			Constant shear displacement amplitude		
		$0.25\tau_p$	$0.50\tau_p$	$0.75\tau_p$	$0.25d_p$	$0.50d_p$	$0.75d_p$
ϕ (Degrees)	40.0	39.5	39.3	38.8	40.0	39.7	38.9
c (MPa)	0.90	0.88	0.84	0.83	0.87	0.85	0.84

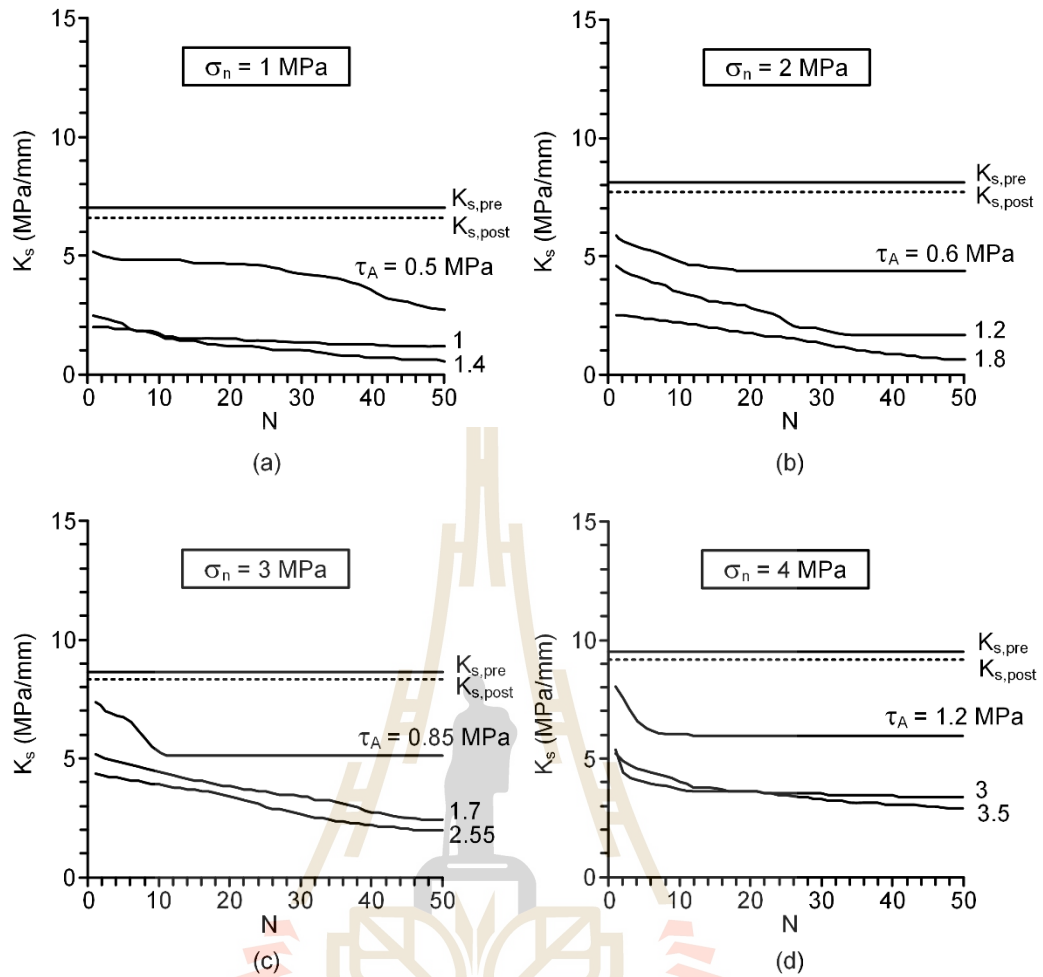


Figure 5.13 Fracture shear stiffness (K_s) as a function of shear cycle (N) for constant shear stress amplitudes under normal stresses of 1 MPa (a), 2 MPa (b), 3 MPa (c) and 4 MPa (d). Solid and dash lines are monotonic loading results of original fractures and of fractures after cyclic loading, respectively.

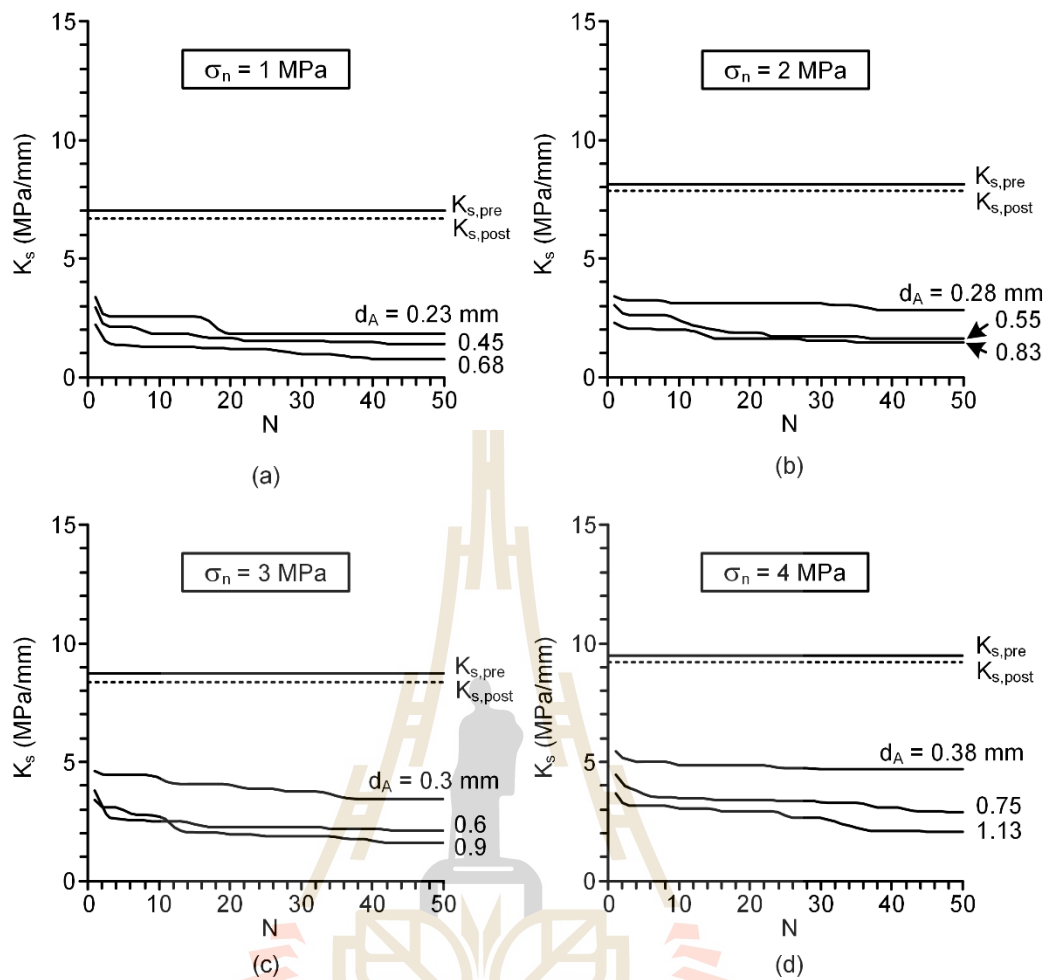


Figure 5.14 Fracture shear stiffness (K_s) as a function of shear cycle (N) for constant shear displacement amplitudes under normal stresses of 1 MPa (a), 2 MPa (b), 3 MPa (c) and 4 MPa (d). Solid and dash lines are monotonic loading results of original fractures and of fractures after cyclic loading, respectively.

5.6 Post-test observation

Figure 5.15 shows the JRC values as a function of normal stress under monotonic loading without cyclic loading and after subjecting to the cyclic loading. The results indicate that the JRC's of monotonic loading after subjecting to the cyclic

loading are lower than those without cyclic loading. The monotonic loading shows clearly that the degradation of fractures under monotonic loading is larger than that cyclic loading. The cyclic loading only affects the second-order asperities, but monotonic loading is mainly governed by the first-order asperities. The cyclic loading under constant shear stress amplitude (CS) can reduce JRC value than those under shear displacement amplitude (CD). This implies that the constant stress amplitude testing can degrade fracture roughness more than the constant displacement amplitude.

Figures 5.16 and 5.17 compare post-test fractures of monotonic loading after cyclic loading under the two test conditions. The results show that higher normal stresses are applied the larger sheared-off areas are obtained. Post-test observations of the sheared fractures shows the sheared-off asperities with slight amount of rock powder deposition under both cyclic loading conditions (Figures 5.7 and 5.11). The fractures of monotonic loading after cyclic loadings show larger sheared-off area than those obtained under monotonic loading without cyclic loading.

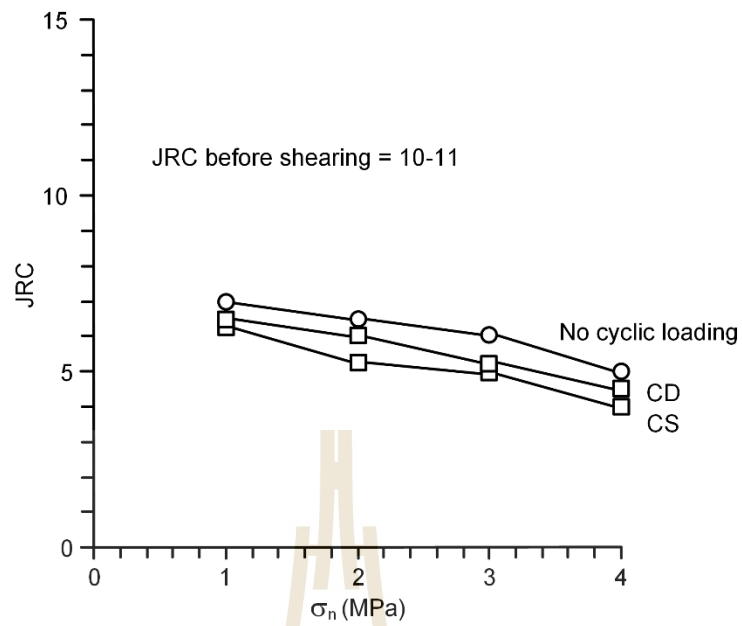


Figure 5.15 JRC's of fractures after monotonic shearing without cyclic loading and after cyclic loading under constant shear stress amplitude (CS) under constant shear displacement amplitude (CD).

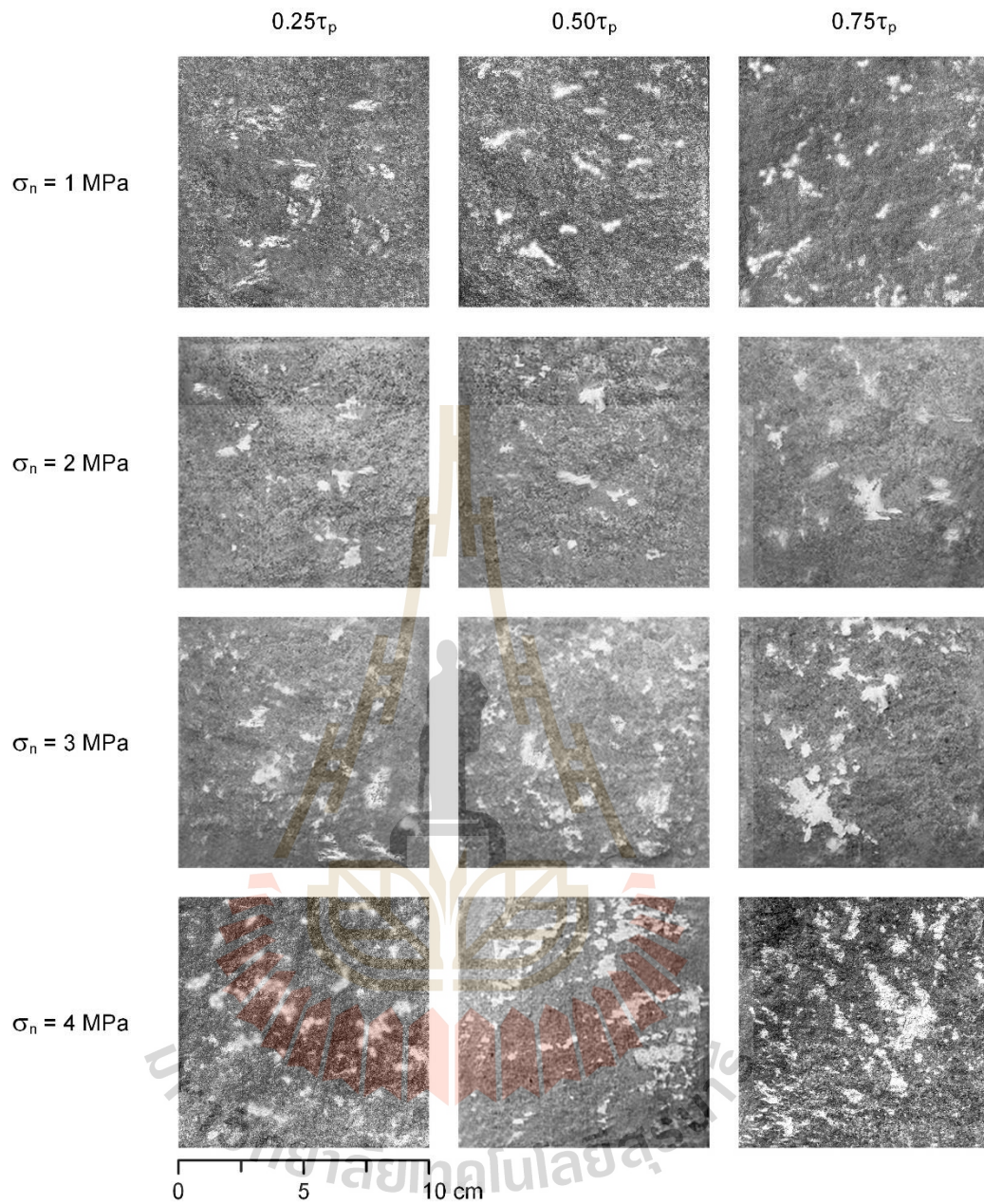


Figure 5.16 Post-test fractures of monotonic loading after cyclic loadings for constant shear stress amplitudes under normal stresses of 1 MPa, 2 MPa, 3 MPa and 4 MPa.

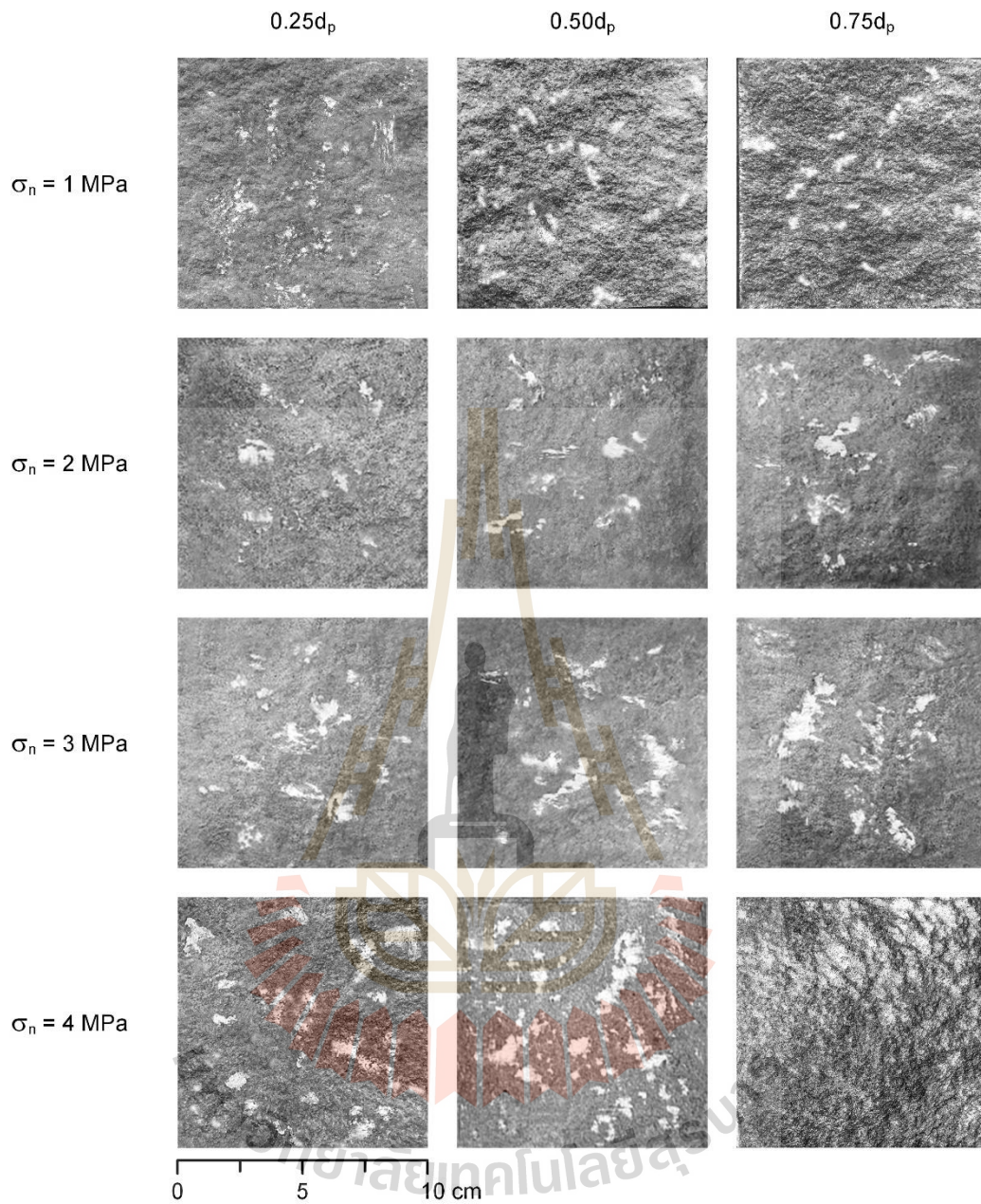


Figure 5.17 Post-test fractures of monotonic loading after cyclic loadings for constant shear displacement amplitudes under normal stresses of 1 MPa, 2 MPa, 3 MPa and 4 MPa.

CHAPTER VI

SHEAR ENERGY

6.1 Introduction

This chapter describes the energy required to shear the fractures under cyclic loading, monotonic loading, and monotonic loading after subjecting to the cyclic loading.

6.2 Shear energy

An attempt is made here to analyze the fracture shear strengths and displacements under cyclic loading by simultaneously considering both shear stress and shear displacement. The shear energy principle proposed by Hutson and Dowding (1990) and Huang et al. (1993) is applied to the test results obtained here. The energy (U) required to shear a rock fracture can be calculated by:

$$U = \sigma_n \cdot d_n + \tau \cdot d \quad (6.1)$$

where σ_n is normal stress and d_n is normal displacement (dilation). Figures 6.1 and 6.2 show the energy (U) calculated for all loading cycles under normal stresses of 1, 2, 3 and 4 MPa for both test conditions. The results indicate that the energy required to reach a constant shear stress amplitude tends to increase with loading cycles (Figure 6.1).

On the other hand, the energy required to reach a constant displacement amplitude tend to decrease with increasing the loading cycles (Figure 6.2). This is primarily because the shear displacement for the constant stress amplitude testing progressively increases with the loading cycles (Figure 5.4) while the shear stress for the constant displacement amplitude testing tends to decrease with increasing loading cycles (Figure 5.5). The diagrams in Figures 6.1 and 6.2 also show that the energy required to monotonically shear the fracture through beyond the peak strength is higher than those required during cyclic loading. The monotonic shearing of the original fractures requires energy (U_{pre}) slightly higher than does the shearing of fractures after cyclic loading (U_{post}). This agrees with the previous observations on the fracture shear strength and shear stiffness given in the previous sections that the cyclic loading peak shear strength of the rock fractures due to the degradation of the second order fracture asperities. Tables 6.1 and 6.2 show the summary of energy for constant stress amplitude and constant displacement amplitude.

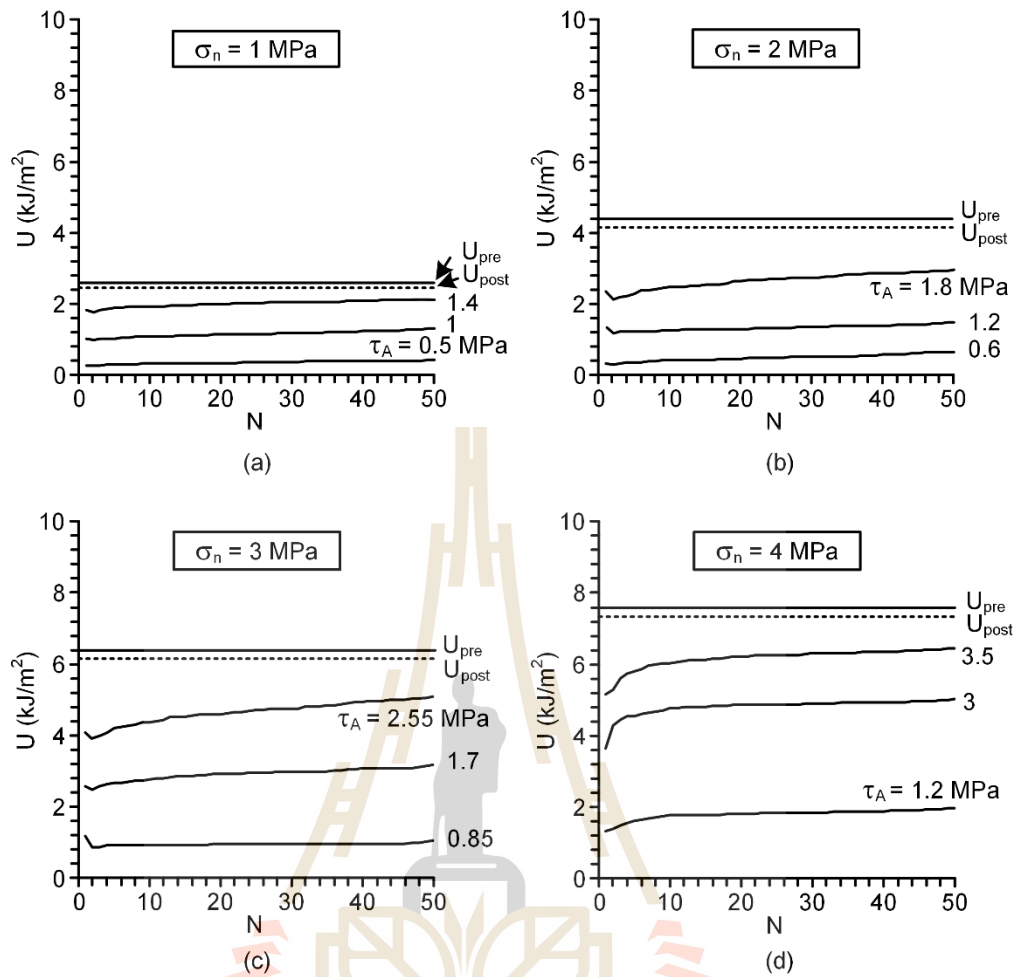


Figure 6.1 Energy (U) as a function of shear cycle (N) for constant shear stress amplitudes under normal stresses of 1 MPa (a), 2 MPa (b), 3 MPa (c) and 4 MPa (d). Solid and dash lines are monotonic loading results of original fractures and of fractures after cyclic loading, respectively.

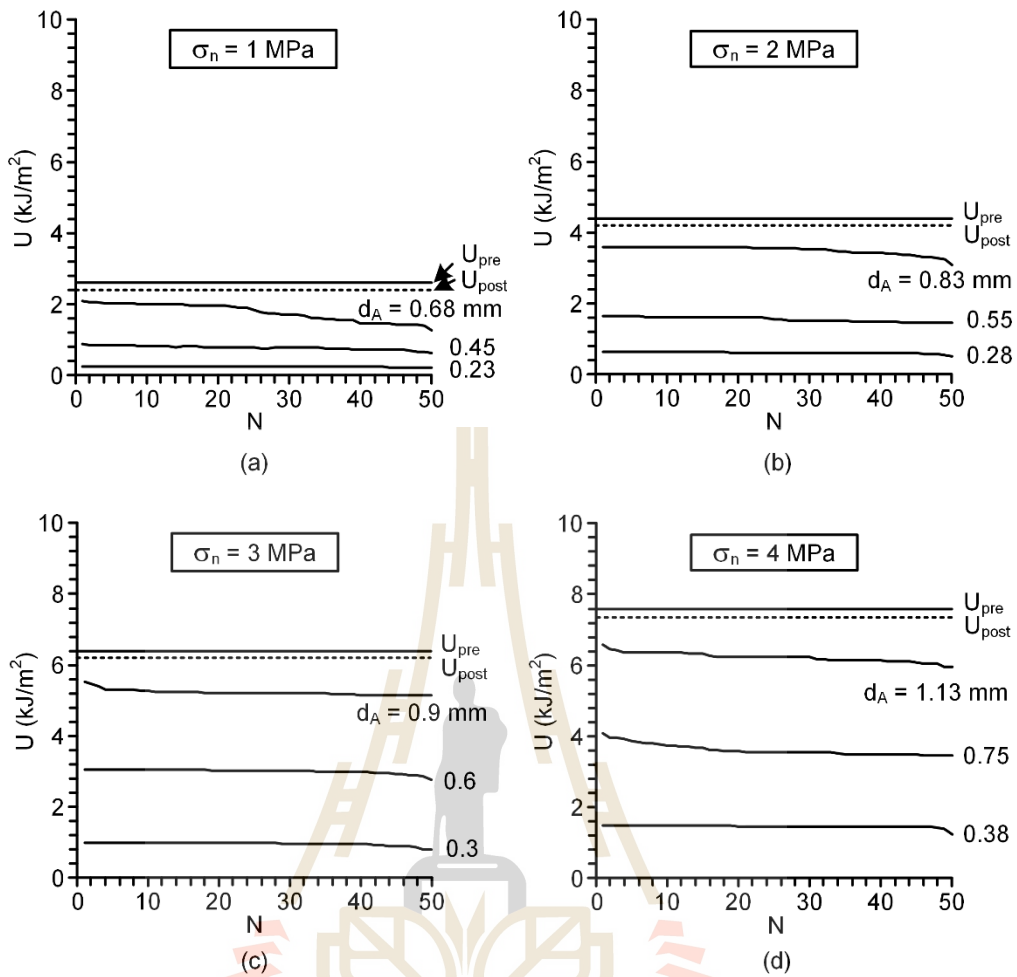


Figure 6.2 Energy (U) as a function of shear cycle (N) for constant shear displacement amplitudes under normal stresses of 1 MPa (a), 2 MPa (b), 3 MPa (c) and 4 MPa (d). Solid and dash lines are monotonic loading results of original fractures and of fractures after cyclic loading, respectively.

Table 6.1 Summary of energy for constant stress amplitude.

σ_n (MPa)	τ			d			d_n			U		
	τ_p (MPa)	τ_A (MPa)	τ_{post} (MPa)	d_p (mm)	d_A (mm)	d_{post} (mm)	$d_{n,p}$ (mm)	$d_{n,A}$ (mm)	$d_{n,post}$ (mm)	U_p (kJ/m ²)	U_A (kJ/m ²)	U_{post} (kJ/m ²)
1	1.80	0.50	1.75	0.85	0.32	0.82	1.07	0.10	0.82	2.60	0.42	2.25
		1.00	1.69		0.55	0.80		0.05	0.88		1.27	2.23
		1.40	1.67		0.65	0.78		0.04	0.91		2.08	2.21
2	2.47	0.60	2.44	1.10	0.44	1.09	0.84	0.11	0.77	4.40	0.68	4.19
		1.20	2.40		0.70	1.07		0.12	0.79		1.55	4.15
		1.80	2.34		0.89	1.05		0.14	0.84		2.94	4.14
3	3.43	0.85	3.40	1.20	0.51	1.14	0.76	0.08	0.77	6.40	1.11	6.20
		1.70	3.36		0.82	1.14		0.15	0.79		3.20	6.19
		2.55	3.29		1.02	1.11		0.20	0.83		5.12	6.15
4	4.27	1.20	4.18	1.50	0.62	1.45	0.30	0.17	0.33	7.60	2.02	7.38
		3.00	4.10		1.00	1.43		0.21	0.37		5.08	7.34
		3.50	4.03		1.10	1.41		0.19	0.41		6.42	7.33

Table 6.2 Summary of energy for constant displacement amplitude.

σ_n (MPa)	τ			d			d_n			U		
	τ_p (MPa)	τ_A (MPa)	τ_{post} (MPa)	d_p (mm)	d_A (mm)	d_{post} (mm)	$d_{n,p}$ (mm)	$d_{n,A}$ (mm)	$d_{n,post}$ (mm)	U_p (kJ/m ²)	U_A (kJ/m ²)	U_{post} (kJ/m ²)
1	1.80	0.31	1.76	0.85	0.23	0.84	1.07	0.03	0.97	2.60	0.20	2.45
		0.41	1.74		0.45	0.84		0.09	0.94		0.61	2.40
		0.83	1.69		0.68	0.83		0.02	0.95		1.23	2.35
2	2.47	0.62	2.44	1.10	0.28	1.08	0.84	0.06	0.82	4.40	0.57	4.27
		1.21	2.41		0.55	1.05		0.09	0.85		1.48	4.23
		1.65	2.36		0.83	1.05		0.08	0.86		3.13	4.19
3	3.43	0.91	3.44	1.20	0.30	1.18	0.76	0.05	0.74	6.40	0.80	6.27
		2.58	3.41		0.60	1.17		0.09	0.75		2.78	6.25
		2.74	3.31		0.90	1.15		0.15	0.81		5.18	6.23
4	4.27	2.02	4.22	1.50	0.38	1.48	0.30	0.05	0.30	7.60	1.22	7.43
		2.23	4.19		0.75	1.45		0.10	0.33		3.44	7.38
		2.93	4.06		1.13	1.44		0.12	0.37		5.96	7.33

CHAPTER VII

DISCUSSIONS, CONCLUSIONS AND RECOMMENDATIONS FOR FUTURE STUDIES

7.1 Discussions

Fifty cycles of loading under both test conditions seem adequate to assess the effects of cyclic shearing on the fracture shear strength and stiffness. This is evidenced by the clear trends of the reduction or enhancement of the fracture shear stiffness (Figures 5.13 and 5.14) and of the energy required to displace the fractures under both test conditions. The results of forward-backward cyclic loading under constant stress amplitudes obtained here agree reasonably well with those of Fathi et al. (2016) and Liu et al. (2018). Their investigators use only forward loading, without backward loading. The forward-backward cyclic loading under constant stress amplitude and particularly under constant displacement amplitude has never been performed anywhere. Due to the complexity of the seismic responses of the rock blocks or mass of rock blocks under in-situ condition, it is believed that the actual movement of these blocks would be governed by the loading characteristics that lie within the two extreme conditions simulated in this study. A significance finding obtained here is that the pre-peak cyclic loading can reduce the rock fracture shear strengths. The shear strength reduction is however small as compared to those of the fractures that are subjected to the post-peak cyclic loading as previously performed by other investigators Hutson and Dowding (1990), Lee et al. (2001), Jafari et al. (2003), and Hosseini et al. (2004).

7.2 Conclusions

All objectives and requirements of this study have been met. The results of the laboratory testing and analyses can be concluded as follows:

(1) The effect of shear displacement under constant shear stress amplitude increases with increasing number of cycles. For constant stress amplitude, the high stress amplitude (75% of peak strength), the shear displacement progresses in the forward direction more than that in the backward direction. This may be due to that the sheared-off rock powder has deposited in the fracture aperture. The larger number of shear cycles, the more rock powder has deposited in the aperture. This phenomenon has not been observed for the lower stress amplitude (25% of peak strength). The shear displacement under monotonic loading of identical fractures (no cyclic loading) are slightly higher than those of the fractures after subjecting to the cyclic loading (Figure 5.4).

(2) The shear strength decreases with increasing number of cycles under constant shear displacement amplitude (Figure 5.8). The shear strength under monotonic loading of identical fractures are slightly higher than those of the fractures after subjecting to the cyclic loading (Figure 5.12).

(3) The friction angles and cohesions decrease with increasing shear stress and displacement amplitudes (Table 5.3). The friction angles and cohesions can decrease by about 1 degree and 0.06 MPa for high stress amplitude ($\tau_A = 1.4$ MPa or 75% of peak strength, τ_p) and high displacement amplitude ($d_A = 1.13$ mm or 75% of d_p).

(4) The fracture shear stiffness (K_s) values for both cyclic test conditions show rapid decreases within the first few cycles due to the degradation of the second order fracture asperities. Fractures under constant stress amplitudes tend to degrade more quickly than those

under constant displacement amplitude. The K_s under monotonic loading after subjecting to cyclic loading is slightly lower than that of the original fractures. This supports the observations that the shear strengths of the fractures after subjecting to cyclic loading are slightly lower than those of the original fractures (Figures 5.13 and 5.14).

(5) The fractures under monotonic loading without cyclic loading and after subjecting to the cyclic loading degrade more than that of the cyclic loading (Figures 5.6 and 5.10). The JRC slightly decreases under cyclic loading test because the cyclic loading only shears the second-order asperities. The monotonic loading is mainly governed by the first-order asperities. The cyclic loading under constant shear stress amplitude can reduce JRC value more than those under shear displacement amplitude. This implies that the constant stress amplitude testing can degrade fracture roughness more than the constant displacement amplitude.

(6) Post-test fractures of monotonic loading after cyclic loading under the two test conditions show that the higher normal stresses are applied the larger sheared-off areas are obtained (Figures 5.16 and 5.17).

(7) The energy required to shear a rock fracture under constant shear stress amplitude tends to increase with loading cycles (Figure 6.1). On the other hand, the energy for the constant displacement amplitude tends to decrease with increasing the loading cycles (Figure 6.2). This is primarily because the shear displacement under constant stress amplitude testing progressively increases with the loading cycles while the shear stress under displacement amplitude testing tends to decrease with increasing loading cycles. The monotonic shearing of the original fractures requires energy slightly higher than does the shearing of fractures after cyclic loading. This agrees with the previous observations on the fracture shear strength and shear stiffness.

(8) The shear strength, friction angle and cohesion slightly decrease under pre-peak cyclic loading. So, the geologic structure should be realizing the initial parameter its design, such as vibration from blasting process in opencast mines.

7.3 Recommendations for future studies

Recognizing that the numbers of the specimens and the test parameters used here are relatively limited, more testing and measurements are recommended, as follows:

(1) Admittedly the conclusions drawn above are limited to one rock type with relatively smooth fractures ($JRC = 10-11$). Obtaining test results on a variety of rock strengths and roughness would likely enhance the reliability of the conclusions drawn here or gain more understanding and knowledge on the fracture shearing behavior under pre-peak cyclic loading.

(2) The fracture areas used in this study ($100 \times 100 \text{ mm}^2$) are relatively small even though they are well complied with the relevant standard practice and internationally suggested method. Testing on larger fracture areas would provide a more representative of the shear strength results when they are applied to the actual fractures under in-situ condition.

(3) The effects of normal stress should be further investigated. In this study the maximum normal stress is 4 MPa. The maximum normal stress used here may not be adequate to truly understand the mechanisms of fault movement. Such high confinement testing however can not be achieved by the normal loading device used in this study. Special and high-loading device is needed for this task.

REFERENCES

- ASTM D5607-08. (2008). **Standard Test Method for Performing Laboratory Direct Shear Strength Tests of Rock Specimens Under Constant Normal Force**. ASTM International, West Conshohocken, PA.
- Barton, N. (1982). Shear strength investigations for surface mining. In **Proceedings of the Third International Symposium on Surface Mining** (pp. 171-196). Canada.
- Brown E.T. (1981). **Rock characterization**. Testing and monitoring-ISRMS suggested methods, Oxford, Pergamon.
- Chern, S.G., Cheng, T.C., and Chen, W.Y. (2012). Behavior of regular triangular joints under cyclic shearing. **Journal of Marine Science and Technology**. 20(5): 508-513.
- Chokchai, B. and Fuenkajorn, K. (2013). Effects of loading rate on joint shear strength in sandstones. In **Proceedings of the Fourth Thailand Symposium on Rock Mechanics** (pp. 297-308). Nakhon Ratchasima, Thailand.
- Fathi, A., Moradian, Z., Rivard, P., and Ballivy, G. (2016). Shear mechanism of rock joints under pre-peak cyclic loading condition. **International Journal of Rock Mechanics and Mining Sciences**. 83: 197-210.

- Fathi, A., Moradian, Z., Rivard, P., Ballivy, G., and Boyd, A.J. (2016). Geometric effect of asperities on shear mechanism of rock joints. **Rock Mechanics and Rock Engineering**, 49(3): 801-820.
- Gentier, S., Riss, J., Archambault, G., Flamand, R., and Hopkins, D. (2000). Influence of fracture geometry on shear behavior. **International Journal of Rock Mechanics and Mining Sciences**. 37(1-2): 161-174.
- Homand, F., Belem, T., and Souley, M. (2001). Friction and degradation of rock joint surfaces under shear loads. **International Journal for Numerical and Analytical Methods in Geomechanics**. 25(10): 973-999.
- Hosseini, K.A., Pellet, F., Jafari, M.K., and Boulon, M. (2004). Shear strength reduction of rock joints due to cyclic loading. In **Proceedings of the Thirteen World Conference on Earthquake Engineering**. Vancouver, Canada.
- Huang, X., Haimson, B.C., Plesha, M.E., and Qiu, X. (1993). An investigation of the mechanics of rock joints-Part I. Laboratory investigation. **International Journal of Rock Mechanics and Mining Sciences & Geomechanics abstracts**. 3: 257-269.
- Hussaini, S.K.K., Indraratna, B. and Vinod, J. S. (2012). Performance of geosynthetically-reinforced rail ballast in direct shear conditions. In **Proceedings of the Eleven Australia-New Zealand Conference on Geomechanics** (pp. 1268-1273). Australia.
- Hutson, R.W. and Dowding, C.H. (1990). Joint asperity degradation during cyclic shear. **International Journal of Rock Mechanics and Mining Sciences & Geomechanics Abstracts**. 27 (2): 109-119.

- Indraratna, B., Mirzaghobanali, A., Oliveira, D.A.F., and Premadasa, W. (2012). Shear behaviour of rock joints under cyclic loading. In **Proceedings of the Eleven Australia-New Zealand Conference on Geomechanics** (pp. 1256-1261). Australia.
- Jafari, M. K., Hosseini, K. A., Pellet, F., Boulon, M., and Buzzi, O. (2003). Evaluation of shear strength of rock joints subjected to cyclic loading. **Soil Dynamics and Earthquake Engineering**. 23(7): 619-630.
- Jing, L., Stephansson, O., and Nordlund, E. (1993). Study of rock joints under cyclic loading conditions. **Rock Mechanics and Rock Engineering**. 26(3): 215-232.
- Johansson, F. (2016). Influence of scale and matedness on the peak shear strength of fresh, unweathered rock joints. **International Journal of Rock Mechanics and Mining Sciences**. 82: 36-47.
- Kamonphet, T., Khamrat, S., and Fuenkajorn, K. (2015). Effects of cyclic shear loads on strength, stiffness and dilation of rock fractures. **Songklanakarinn Journal of Science and Technology**. 37(6): 683-690.
- Khamrat, S., Archeeploha, S., and Fuenkajorn, K. (2016). Pore pressure effects on strength and elasticity of ornamental stones. **Scienceasia**. 42: 121-135.
- Lee, H.S., Park, Y.J., Cho, T.F., and You, K.H. (2001). Influence of asperity degradation on the mechanical behavior of rough rock joints under cyclic shear loading. **International Journal of Rock Mechanics and Mining Sciences**. 38(7): 967-980.
- Liu, X.R., Kou, M.M., Lu, Y.M., and Liu, Y.Q. (2018). An experimental investigation on the shear mechanism of fatigue damage in rock joints under pre-peak cyclic loading condition. **International Journal of Fatigue**. 106: 175-184.

- Ma, M. and Brady, B.H. (1999). Analysis of the dynamic performance of an underground excavation in jointed rock under repeated seismic loading. **Geotechnical & Geological Engineering**. 17(1): 1-20.
- Mirzaghobanali, A., Nemcik, J., and Aziz, N. (2014). Effects of shear rate on cyclic loading shear behaviour of rock joints under constant normal stiffness conditions. **Rock mechanics and rock engineering**. 47(5): 1931-1938.
- Misra, A. (2002). Effect of asperity damage on shear behavior of single fracture. **Engineering Fracture Mechanics**. 69(17): 1997-2014.
- Niktabar, S.M., Rao, K.S., and Shrivastava, A. K. (2017). Effect of rock joint roughness on its cyclic shear behavior. **Journal of Rock Mechanics and Geotechnical Engineering**. 9(6): 1071-1084.
- Prasetyo, S.H., Gutierrez, M., and Barton, N. (2017). Nonlinear shear behavior of rock joints using a linearized implementation of the Barton-Bandis model. **Journal of Rock Mechanics and Geotechnical Engineering**. 9(4): 671-682.
- Puntel, E., Bolzon, G., and Saouma, V. E. (2006). Fracture mechanics based model for joints under cyclic loading. **Journal of engineering mechanics**. 132(11): 1151-1159.
- Souley, M., Homand, F., and Amadei, B. (1995). An extension to the Saeb and Amadei constitutive model for rock joints to include cyclic loading paths. **International Journal of Rock Mechanics and Mining Sciences & Geomechanics Abstracts**. 101-109.
- Tang, Y. and Ranjith, P.G. (2018). An experimental and analytical study of the effects of shear displacement, fluid type, joint roughness, shear strength, friction angle and dilation angle on proppant embedment development in tight gas sandstone

reservoirs. **International Journal of Rock Mechanics and Mining Sciences**. 107: 94-109.

Wang, G., Zhang, X., Jiang, Y., Wu, X., and Wang, S. (2016). Rate-dependent mechanical behavior of rough rock joints. **International Journal of Rock Mechanics and Mining Sciences**. 83: 231-240.

Zhao, J. (1997). Joint surface matching and shear strength part B: JRC-JMC shear strength criterion. **International Journal of Rock Mechanics and Mining Sciences**. 34(2): 179-185.



BIOGRAPHY

Mr. Narudon Patitung was born on October 10, 1994 in Nakhon Ratchasima province, Thailand. He received his Bachelor's Degree in Engineering (Geotechnology) from Suranaree University of Technology in 2017. For his post-graduate, he continued to study with a Master's degree in the Geological Engineering Program, Institute of Engineering, Suranaree university of Technology. During graduation, 2017-2019, he was a part time worker in position of research assistant at the Geomechanics Research Unit, Institute of Engineering, Suranaree University of Technology.

